Supplementary Information

Roboticized AI-assisted microfluidic photocatalytic synthesis and screening up to 10,000 reactions per day

Jia-Min Lu[1,2,7], Hui-Feng Wang[1,2,7], Qi-Hang Guo[1,2,3,7], Jian-Wei Wang[2], Tong-Tong Li[1,3], Ke-Xin Chen[4,5], Meng-Ting Zhang[1], Jian-Bo Chen[1], Qian-Nuan Shi[2], Yi Huang[2], Shao-Wen Shi[2], Guang-Yong Chen[4,*], Jian-Zhang Pan[1,2,*], Zhan Lu[1,3,*], Qun Fang[1,2,6,*]

[1] Department of Chemistry, Zhejiang University, Hangzhou 310058, China

[2] Institute of Intelligent Chemical Manufacturing and iChemFoundry Platform, ZJU-Hangzhou Global Scientific and Technological Innovation Center, Hangzhou 311200, China

[3] Center of Chemistry for Frontier Technologies, Department of Chemistry, Zhejiang University, Hangzhou 310058, China

[4] The Research Center for Life Sciences Computing, Zhejiang Lab, Hangzhou 311121, China

[5] Department of Computer Science and Engineering, The Chinese University of Hong Kong, New Territories, Hong Kong SAR 000000, China

[6] Key Laboratory of Excited-State Materials of Zhejiang Province, Zhejiang University, Hangzhou 310058, China

[7] These authors contributed equally.

Corresponding author: fangqun@zju.edu.cn; luzhan@zju.edu.cn; kelvonpan@zju.edu.cn; gychen@zhejianglab.com

Table of Contents

1. Materials and methods of photocatalytic [2+2] cycloaddition

Starting materials and other reagents of the photocatalytic [2+2] cycloaddition were prepared according to the following procedures[1].

$Ir(dFCF_3ppy)_2(dtbbpy)(PF_6)$ (**Ir-1**) was prepared according to a reported procedure[2]. $Ir(dFMeppy)_2(dtbbpy)(PF_6)$ (**Ir-2**) was prepared according to a reported procedure[3]. $Ir(dFCF_3ppy)_2(bpy)(PF_6)$ (**Ir-3**) was prepared according to a reported procedure[4]. $Ir(dFMeppy)_2(bpy)(PF_6)$ (**Ir-4**) was prepared according to a reported procedure[5]. $Ir(ppy)_3$ (**Ir-5**) was prepared according to a reported procedure[6]. THF, toluene, 1,4-dioxane, and diethyl ether were distilled from sodium benzophenoneketyl prior to use. CH_3CN, iPr_2NEt, C_6F_6 and DME were distilled from CaH_2. Sodium hydride (NaH) and methylmagnesium bromide were purchased from Energy and used as received. The other commercially available chemicals were used as received if not mentioned otherwise. NMR spectra were recorded on a Bruker-400 instrument or Oxford instrument. ^1H NMR chemical shifts were referenced to tetramethylsilane signal (0 ppm), ^{13}C NMR chemical shifts were referenced to the solvent resonance (77.00 ppm, $CDCl_3$), ^{19}F NMR chemical shifts were referenced to the solvent resonance. The following abbreviations (or combinations thereof) were used to explain multiplicities: s = singlet, d = doublet, t = triplet, m = multiplet, br = broad, q = quadruplet, PE = petroleum ether, EA = ethyl acetate, THF = tetrahydrofuran, DCM = dichloromethane. IR spectra were recorded on a Perkin-Elmer Spectrum One FTIR spectrometer with diamond ATR accessory. High-resolution mass spectra (HRMS) were recorded on LCMS-IT-TOF (ESI-TOF) and EI-TOF (electro-spray ionization-time of flight) mass spectrometers. Melting points were measured using an X-4 melting point apparatus (Laboratory Devices, Beijing Taike Co., Beijing, China).

Starting materials were prepared by the following step[1]:

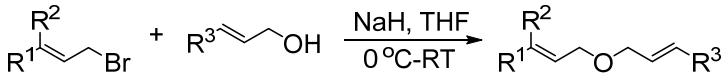

A flame-dried 100 mL three-necked flask was charged with 60% NaH (1.2 equiv) and dry THF (1 M). Alcohol (1.0 equiv) in THF (1 M) was added dropwise, and the reaction was stirred for an additional 30 min at room temperature. The flask was then cooled to 0 °C, and a solution of allyl bromide (1.2 equiv) in THF (1 M) was added dropwise. The mixture was allowed to warm up to room temperature. After stirring for 12 h, the reaction was quenched by addition of saturated NH_4Cl. The mixture was separated, and the aqueous phase was extracted three times with DCM. The combined organic phases were then washed with brine, dried over Na_2SO_4, and concentrated by rotary evaporation. The residue was purified by flash-column chromatography using 40:1 hexanes/ethyl acetate as the eluent to afford the corresponding product **S**.

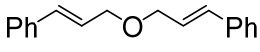

((1*E*,1′*E*)-Oxybis(prop-1-ene-3,1-diyl))dibenzene (S-1): 19.51 g, 78% yield, white soild, ^{1}H NMR: (400 MHz, $CDCl_3$) δ 7.40 (d, *J* = 7.4 Hz, 4H), 7.32 (dd, *J* = 7.4, 7.8 Hz, 4H), 7.27-7.20 (m, 2H), 6.64 (d, *J* = 16.0 Hz, 2H), 6.39-6.27 (m, 2H), 4.21 (dd, *J* = 6.0, 1.2 Hz, 4H); analytical data were consistent with previously reported procedure[1].

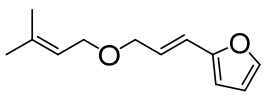

(*E*)-2-(3-((3-Methylbut-2-en-1-yl)oxy)prop-1-en-1-yl)furan (S-2): 6.68 g, 39% yield, light yellow oil, ^{1}H NMR: (400 MHz, $CDCl_3$) δ 7.34 (s, 1H), 6.43 (d, *J* = 16.0 Hz, 1H), 6.36 (s, 1H), 6.30-6.17 (m, 2H), 5.42-5.33 (m, 1H), 4.10 (d, *J* = 6.0 Hz, 2H), 4.00 (d, *J* = 6.8 Hz, 2H), 1.76 (s, 3H), 1.68 (s, 3H); analytical data were consistent with previously reported procedure[1].

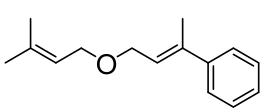

(*E*)-(4-((3-Methylbut-2-en-1-yl)oxy)but-2-en-2-yl)benzene (S-3): 12.87 g, 83% yield, colorless oil, ^{1}H NMR: (400 MHz, $CDCl_3$) δ 7.38-7.27 (m, 4H),

7.25-7.17 (m, 1H), 6.51 (s, 1H), 5.45-5.36 (m, 1H), 4.02 (s, 2H), 3.99 (d, *J* = 6.8 Hz, 2H), 1.90 (s, 3H), 1.77 (s, 3H), 1.69 (s, 3H); analytical data were consistent with previously reported procedure[1].

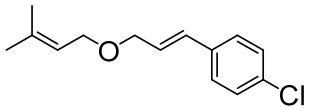

(*E*)-1-Chloro-4-(3-((3-methylbut-2-en-1-yl)oxy)prop-1-en-1-yl)benzene (S-4): 15.11 g, 76% yield, colorless oil, ^{1}H NMR: (400 MHz, $CDCl_3$) δ 7.34-7.25 (m, 4H), 6.56 (d, *J* = 16.0 Hz, 1H), 6.34-6.23 (m, 1H), 5.44-5.34 (m, 1H), 4.12 (d, *J* = 6.0 Hz, 2H), 4.02 (d, *J* = 6.8 Hz, 2H), 1.76 (s, 3H), 1.69 (s, 3H); analytical data were consistent with previously reported procedure[1].

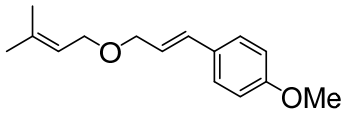

(*E*)-1-methoxy-4-(3-((3-methylbut-2-en-1-yl)oxy)prop-1-en-1-yl)benzene (S-5): 7.36 g, 56% yield, colorless oil, ^{1}H NMR: (400 MHz, $CDCl_3$) δ 7.32 (d, *J* = 8.8 Hz, 2H), 6.85 (d, *J* = 8.8 Hz, 2H), 6.55 (d, *J* = 16.0 Hz, 1H), 6.23-6.11 (m, 1H), 5.44-5.34 (m, 1H), 4.11 (d, *J* = 6.0 Hz, 2H), 4.01 (d, *J* = 6.8 Hz, 2H), 3.80 (s, 3H), 1.76 (s, 3H), 1.68 (s, 3H); analytical data were consistent with previously reported procedure[1].

2. Supplementary figures and tables of the robotic system

LCW photocatalytic microreactor module

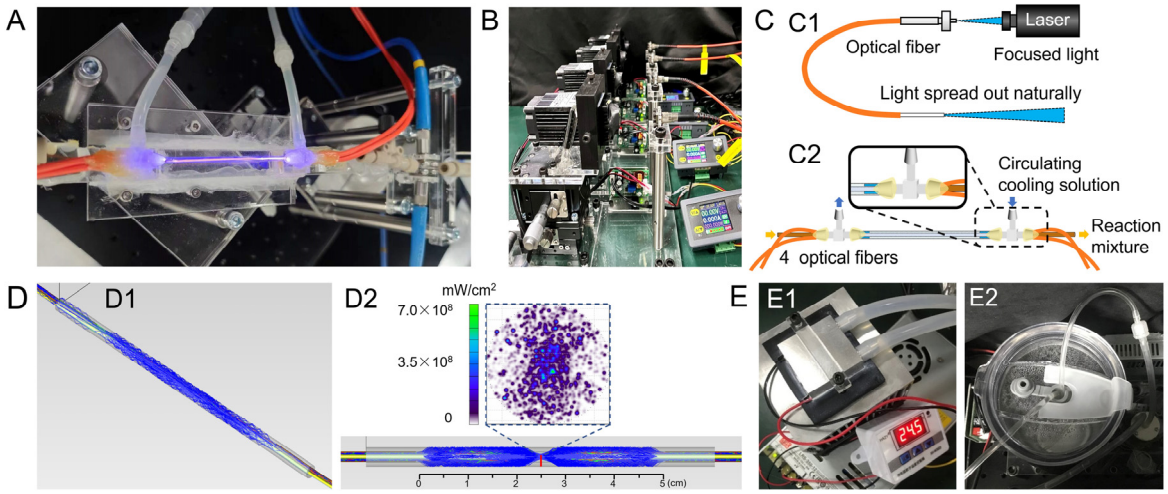

Fig. S1. Structure and performance of the LCW photocatalytic microreactor module. (A) Photograph of the cannula configuration of the LCW photocatalytic microreactor. (B) Photograph of the lasers and optical fibers for optical coupling. (C) Schematic diagram of light coupling from lasers to optical fibers (C1) and from optical fibers to the LCW photocatalytic microreactor (C2). (D) Simulation of light intensity distribution in the LCW photocatalytic microreactor (D1) and in the cross-section of reaction channel (D2) using TracePro software. (E) Temperature controlling device with a digital temperature controller and a semiconductor chilling plate (E1) to monitor and to control the temperature of the cooling solution circulated in the outer capillary which was driven by a diaphragm pump (E2).

Liquid handling module

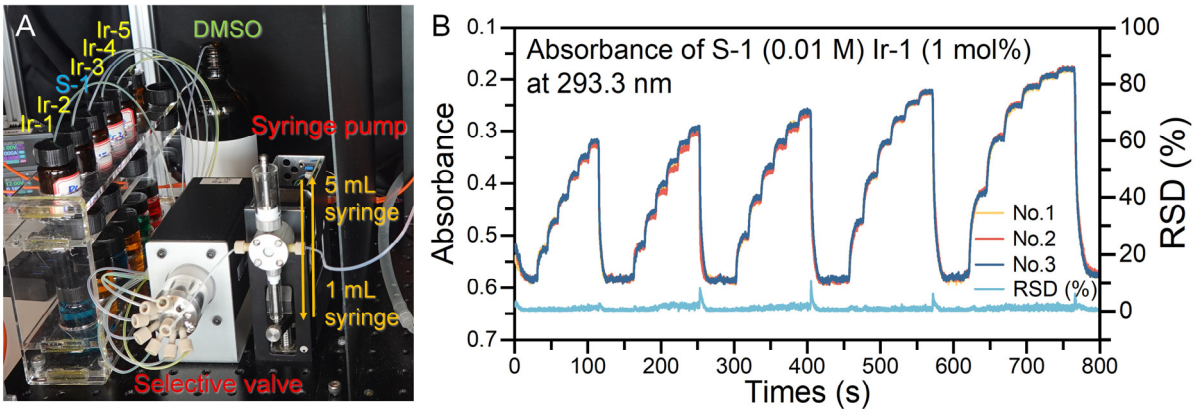

Fig. S2. Setup and stability of the liquid handling module. (A) Photograph of the setup including the 10-port selective valve and the syringe pump for automated condition screening. (B) A set of 30 steady-state absorbance data for S-1 catalyzed by Ir-1 obtained in three repetitions of the experiment. The relative standard deviations (RSD) of the absorbance signal at each time point were below 5% (n = 3) in the three replicate experiments.

Online UV-Vis absorption spectroscopy module

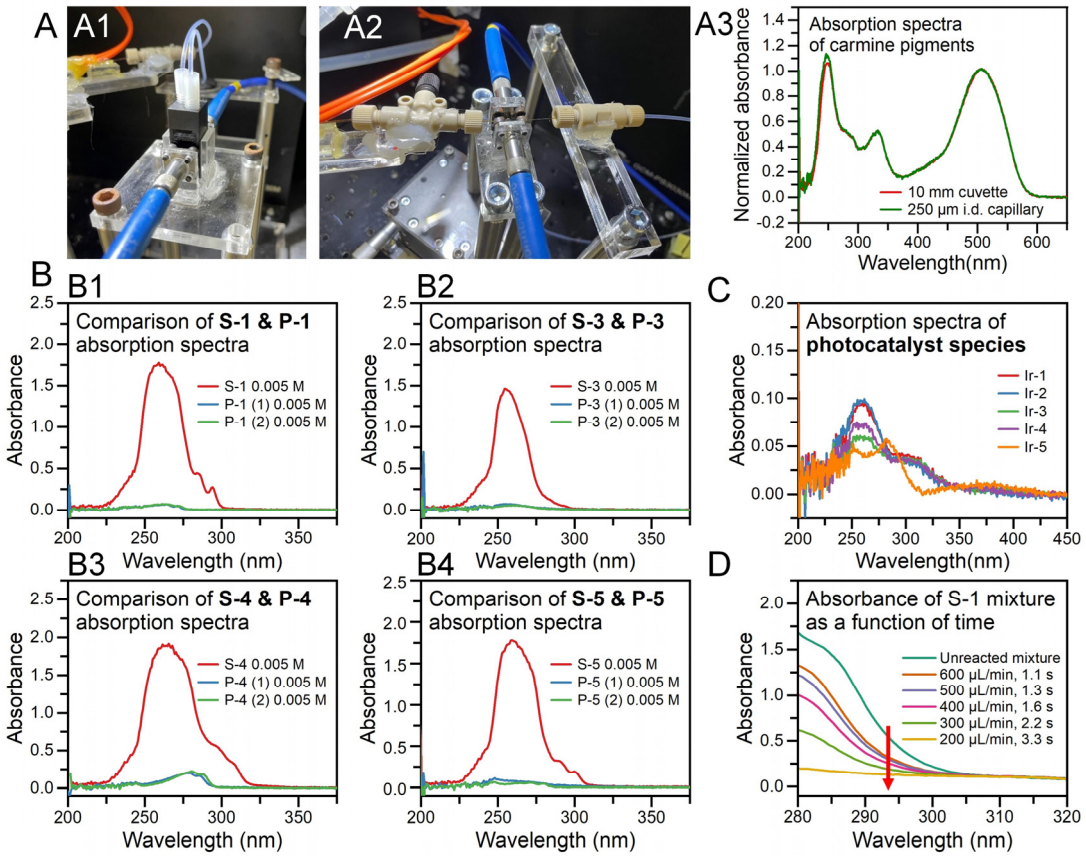

Fig. S3. Feasibility validation of the UV-Vis absorption spectroscopy module for online monitoring of the photocatalytic [2+2] cycloaddition reaction. (A1, A2) Setups used in the validation experiments for the online UV-Vis absorption spectroscopy analytical method using the 10 mm cuvette (A1) and the 250 μm detection capillary (A2); (A3) The absorption spectra of carmine pigment obtained using these two detection vessels in A1 and A2. (B) Absorption spectra of the substrates and the products species, including those of substrate S-1 and corresponding products P-1 (B1), substrate S-3 and corresponding products P-3 (B2), substrate S-4 and corresponding products P-4 (B3), substrate S-5 and corresponding products P-5 (B4). (C) Absorption spectra of photocatalyst species including Ir-1, Ir-2, Ir-3, Ir-4, and Ir-5. (D) Absorption spectra change of the reaction mixtures of S-1 catalyzed by Ir-1 at different flow rates.

AI-assisted prediction of the steady-state absorbance data from the non-steady-state absorbance data.

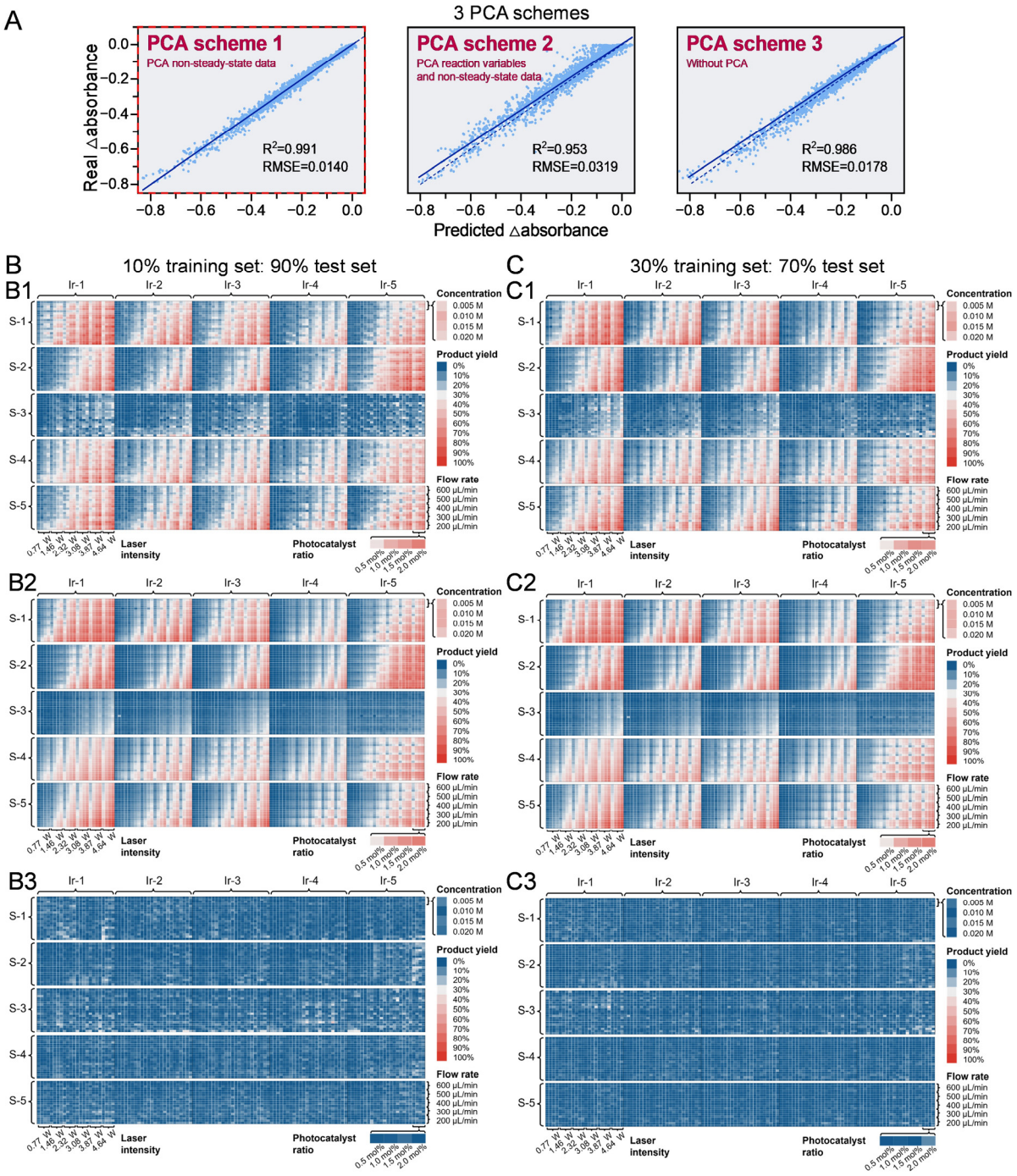

Fig. S4. AI-assisted prediction of the absorbance data and heatmap visualization of product yields. (A) Three PCA schemes for downscaling the original eigenvalues using the XGB model, with the dataset divided into training and test sets with a proportion of 70% and 30%. (B) The heatmaps of the product yields converted from the non-steady-state absorbance data (B1), the steady-state absorbance data (B2), and the absolute errors between them (B3), with the dataset divided into training and test sets with a proportion of 10% and 90%. (C) The heatmaps of the product yields converted from the non-steady-state absorbance data (C1), the steady-state absorbance data (C2), and the absolute errors between them (C3), with the dataset divided into training and test sets with a proportion of 30% and 70%. The product yields are displayed in color gradient with blue indicating low product yields, and red indicating high yields.

Descriptor and algorithms used in AI-assisted cross-species prediction

Table S1. SMILES strings for all the substrate and photocatalyst species.

Substrate species	Substrate (SMILES)	Photocatalyst species	Photocatalyst (SMILES)
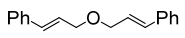	C1(/C=C/COC/C=C/C2=CC=CC=C2)=CC=CC=C1	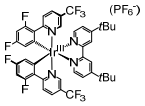	FC(F)(C1=CN=C(C=C1)C2=C(F)C=C(F)C=[C-]2)F.F[P-](F)(F)(F)(F)F.CC(C)(C3=CC(C4=CC(C(C)(C)C)=CC=N4)=NC=C3)C.FC5=CC(F)=C([C-]=C5)C6=NC=C(C=C6)C(F)(F)F.[Ir+3]
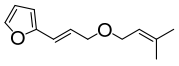	C/C(C)=C/COC/C=C/C1=CC=CO1	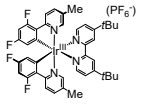	FC1=CC(F)=C(C2=[N]3C=C(C)C=C2)C([Ir]435([N]6=C(C(C5=CC(F)=C7)=C7F)C=CC(C)=C6)[N]8=CC=C(C(C)(C)C)C=C8C9=[N]4C=CC(C(C)(C)C)=C9)=C1.F[P-](F)(F)(F)(F)F
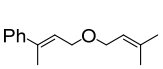	C/C(C)=C/COC/C=C(C)/C1=CC=CC=C1	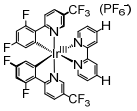	FC1=CC(F)=C(C2=[N]3C=C(C(F)(F)F)C=C2)C([Ir]435([N]6=C(C(C5=CC(F)=C7)=C7F)C=CC(C(F)(F)F)=C6)[N]8=CC=C([H])C=C8C9=[N]4C=CC([H])=C9)=C1.F[P-](F)(F)(F)(F)F
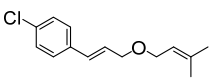	C/C(C)=C/COC/C=C/C1=CC=C(Cl)C=C1	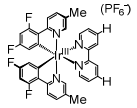	FC1=CC(F)=C(C2=[N]3C=C(C)C=C2)C([Ir]435([N]6=C(C(C5=CC(F)=C7)=C7F)C=CC(C)=C6)[N]8=CC=C([H])C=C8C9=[N]4C=CC([H])=C9)=C1.F[P-](F)(F)(F)(F)F
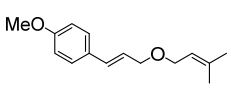	C/C(C)=C/COC/C=C/C1=CC=C(OC)C=C1	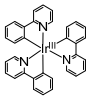	C12=CC=CC=C1C3=[N]([Ir]245(C6=C(C7=CC=CC=[N]75)C=CC=C6)C8=CC=CC=C8C9=[N]4C=CC=C9)C=CC=C3

3. Measurement of laser light intensity

The reactions were carried out with irradiation from 4 blue lasers, and the light was coupled and conducted into the LCW photocatalytic microreactor through 4 quartz optical fibers. To measure the laser light intensity coupled into the LCW photocatalytic microreactor, we replaced each of the 4 optical fibers with another optical fiber that was not connected to the microreactor, and measured the light intensity at its output end by a laser power meter (LP1, Sanwa, Tokyo, Japan) (Fig. S5).

The laser current was set to 0.3 A to make it output weak light that was able to be measured. The position and the focus of the 4 lasers were fine-tuned until all the coupling ratios exceeded 70%, then the actual light intensity could be measured by setting different current using the adjustable power supply (WZ5005E, Xinyue, Qingdao, China). Since the maximum laser light intensity was beyond the test range of the laser power meter whose detection area was 1 cm^2, we enlarged the light spot to detect the local light intensity, and then the total laser light intensity was calculated. By extending the distance between the laser power meter and the optical fiber to 17 cm, the actual area of the light spot at the measurement position was c.a. 20 cm^2. In addition, the measured signal of the laser power meter at 450 nm should be multiplied by a factor of 3.29 to obtain the actual laser light intensity value. Therefore, the total laser light intensity coupled into the LCW microreactor is equal to the laser power meter reading multiplied by an area of 20 cm^2 and a factor of 3.29. With this method, the total laser light intensity of the four lasers coupled into the LCW photocatalytic microreactor was measured to be 4.64 W, as shown in Table S2.

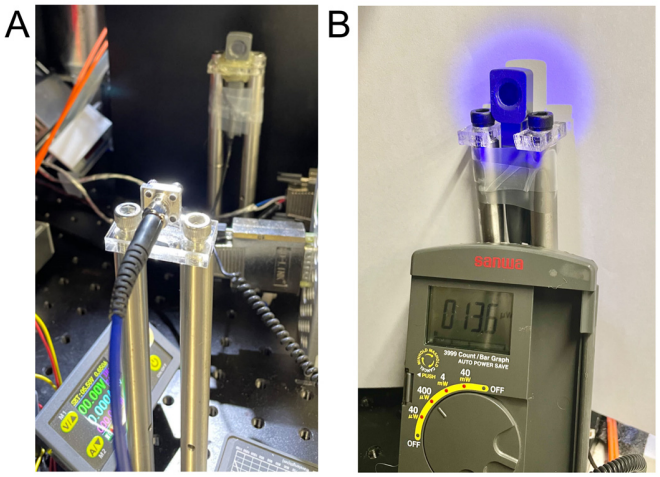

Fig. S5. Photographs of the setup for the laser light intensity measurement. (A) Setup including an optical fiber and a laser power meter. (B) Amplified 20 cm^2 laser light spot for measurement of the light intensity.

Table S2. Coupling ratios and laser light intensity at different currents

Entry	Laser 1 (W)	Laser 2 (W)	Laser 3 (W)	Laser 4 (W)	Laser light intensity (W)
Coupling ratio	73%	71%	71%	71%	-
0.65 A (25% light)	0.30	0.10	0.28	0.09	0.77
0.80 A (40% light)	0.50	0.22	0.52	0.22	1.46
0.95 A (55% light)	0.72	0.4	0.78	0.38	2.32
1.10 A (70% light)	0.94	0.60	1.02	0.52	3.08
1.25 A (85% light)	1.15	0.78	1.26	0.68	3.87
1.40 A (100% light)	1.36	0.95	1.49	0.84	4.64

4. Control program

All modules of the robotic system were automatically controlled by a self-designed LabVIEW-based program (LabVIEW 8.0, National Instruments, Austin, USA), which was capable of controlling

the operation of the selective valves, the syringe pumps, the adjustable power supplies, and the spectrometers, with flexibility to expand the number of each according to the requirements of photocatalytic, electrocatalytic, or photo-electrocatalytic synthesis (Fig. S6). For the condition screening of photocatalytic [2+2] cycloaddition, this program was used to control the specific valve positions of the 10-port selective valve to select different components, as well as the valve positions (3 valve positions in total), the operation modes (e.g., aspiration and dispensing), the flow rates, and the sampling volumes of the syringe pump. In order to control the laser light intensity, the current output of the adjustable power supply could also be set through this control program. For online detection module, we set the acquisition time and number of data smoothing times for UV-Vis absorption spectra recording via the program.

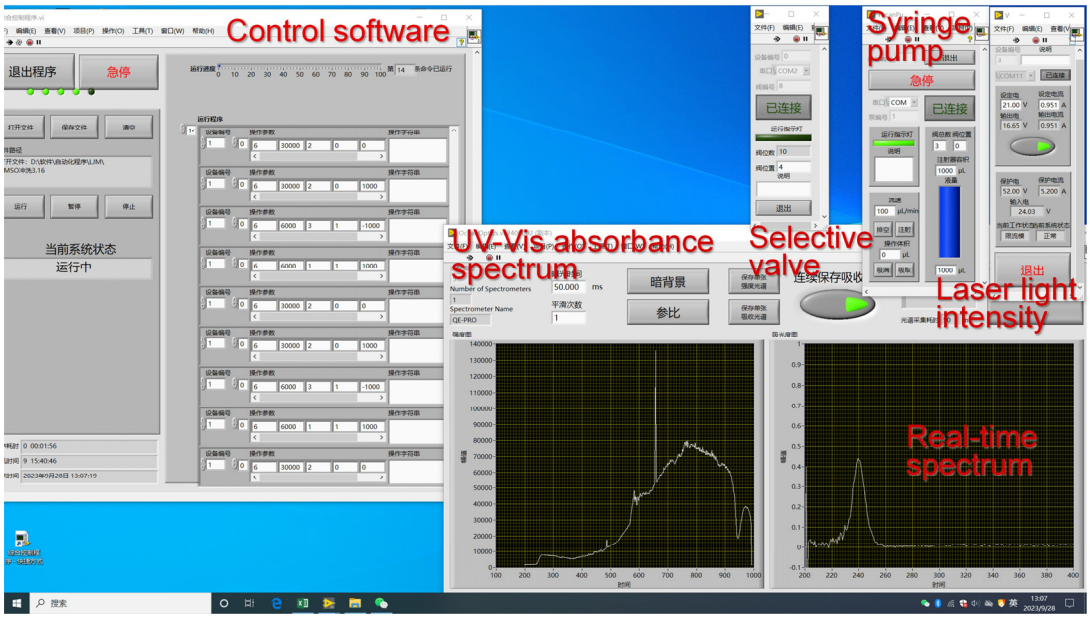

Fig. S6. Self-designed control program for the robotic system in condition screening of the photocatalytic [2+2] cycloaddition. The program could control the operation of a 10-port selective valve, a syringe pump, an adjustable power supply for laser intensity regulation, and a spectrophotometer for UV-Vis absorption spectra recording.

5. Condition screening programming and rapid data processing

A total orthogonal screening for the photocatalytic [2+2] cycloaddition including 12,000 conditions was designed for both continuous and discrete variables, which was difficult to be achieved in conventional organic synthesis experiments owing to the excessive experimental workload. With the robotic system, both steady-state and non-steady-state absorbance data were obtained for all 12,000 screening conditions. In order to increase the throughput and reduce the time for sample switching and channel cleaning, we rationalized the order of condition screening. First, based on the tested substrate species, photocatalyst species, substrate concentration, and photocatalyst ratio, the stock solutions were selected and 5 mL of reaction mixture was prepared according to the steps described in Section 2.2, which was used to screen 30 conditions involving 5 flow rates and 6 laser light intensity in one set of experiments (Fig. S7A1). After that, the conditions of different photocatalyst ratios (i.e., from 0.5 mol% to 2.0 mol%) and different substrate concentrations (i.e., from 0.005 M to 0.02 M) were screened. When all 480 conditions for this substrate and this photocatalyst species (e.g., substrate S-1 and photocatalyst Ir-1) had been screened, the syringe pump, reaction channel of LCW photocatalytic microreactor, and detection flow-cell channel were thoroughly cleaned using the solvent DMSO to avoid cross-contamination. Subsequently, we continued to screen the conditions for this substrate with other photocatalyst species (e.g., substrate S-1 and photocatalyst Ir-2) until all 2400 data for substrate S-1 were obtained.

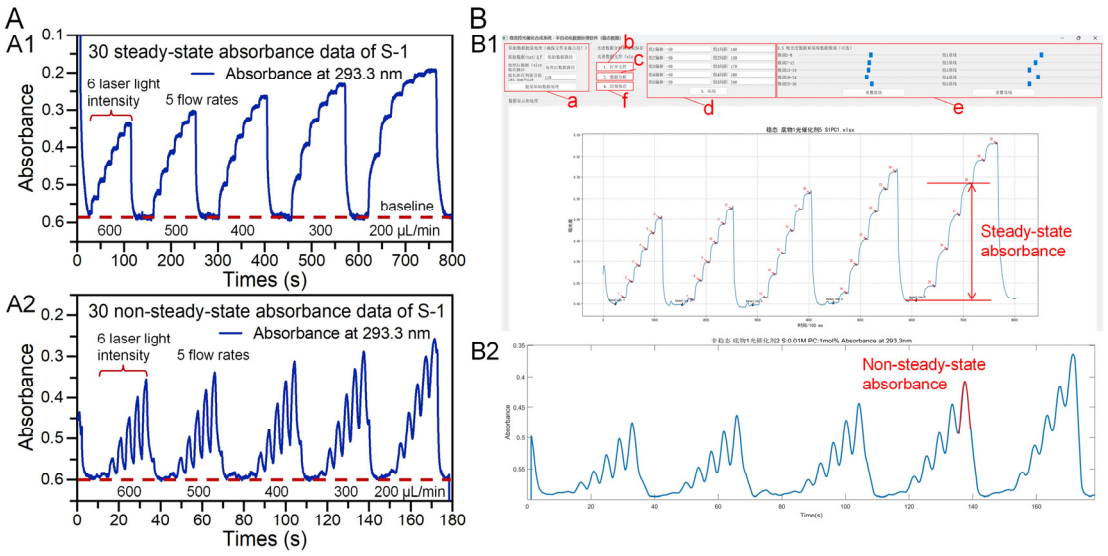

Fig. S7. Typical recordings of steady-state and non-steady-state absorbance data. (A) Typical recordings of 30 conditions involving 5 flow rates and 6 laser light intensity of the steady-state (A1) and non-steady-state (A2) absorbance data for S-1. (B) Self-designed data processing software and method for extracting the steady-state (B1) and the non-steady-state absorbance data (B2).

Unlike the steady-state mode in which the light source was kept on continuously until stable absorbance value was obtained, the light source in the non-steady-state mode repeated the pulse "on (2 s) -off (2 s)" mode for all data acquisition while the reaction mixture flowed continuously through the reaction channel and the detection flow-cell channel. Such a non-steady-state pulse on/off operation mode belongs to the flow injection analysis (FIA) working format, which could dramatically reduce the time for acquiring the peak signals corresponding to the experimental conditions, with the average time for each condition screening shortened from 32 s to 8.5 s (Fig. S7A2). As the reaction proceeded, the difference between the absorbance of unreacted and reacted mixture at the selected wavelength was acquired as the steady-state absorbance data, which was used to primary evaluate the progress and the product yields of the photocatalytic [2+2] cycloaddition

reaction (Fig. S7B1). We designed a data processing program to quickly processing the steady-state absorbance data as well as the non-steady-state absorbance data obtained in the screening experiments (Fig. S7B2).

6. GC and NMR quantitative characterization methods

In order to examine the reliability of the online UV-Vis absorption spectroscopy method in reaction monitoring, we also collected representative reacted mixture solution and quantitatively analyzed them with GC or NMR methods.

It should be noted that the product yields of P-2 were obtained through NMR detection with TMSPh used as the internal standard, while all other product yields were obtained through GC detection. The GC temperature programs were optimized for different substrate species and corresponding products. For accurate quantification, the two products obtained from each substrate species were collected separately using column chromatography. The GC standard curves of the substrates and products were plotted respectively using the internal standard method, with 1-nonanol for substrates S-1, S-3 and S-4 and the corresponding products P-1, P-3 and P-4, while 1-tetradecanol for substrate S-5 and the corresponding products P-5 (Fig. S8).

A GC method and standard curves for S-1 and P-1

A1

	Rate [℃/min]	Temperature [℃]	Hold time [min]	Running time [min]
Start	-	60	1	1
ramp1	5	105	0	10
ramp2	40	220	1	13.9
ramp3	8	240	1	17.4

B GC method and standard curves for S-3 and P-3

B1

	Rate [℃/min]	Temperature [℃]	Hold time [min]	Running time [min]
Start	-	60	1	1
ramp1	5	105	1	11
ramp2	40	170	1	13.6
ramp3	10	190	1	16.6

C GC method and standard curves for S-4 and P-4

C1

	Rate [℃/min]	Temperature [℃]	Hold time [min]	Running time [min]
Start	-	60	1	1
ramp1	5	105	1	11
ramp2	20	180	3	17.8
ramp3	3	190	1	22.1

D GC method and standard curves for S-5 and P-5

D1

	Rate [℃/min]	Temperature [℃]	Hold time [min]	Running time [min]
Start	-	60	1	1
ramp1	60	200	1	4.3
ramp2	10	220	1	7.3

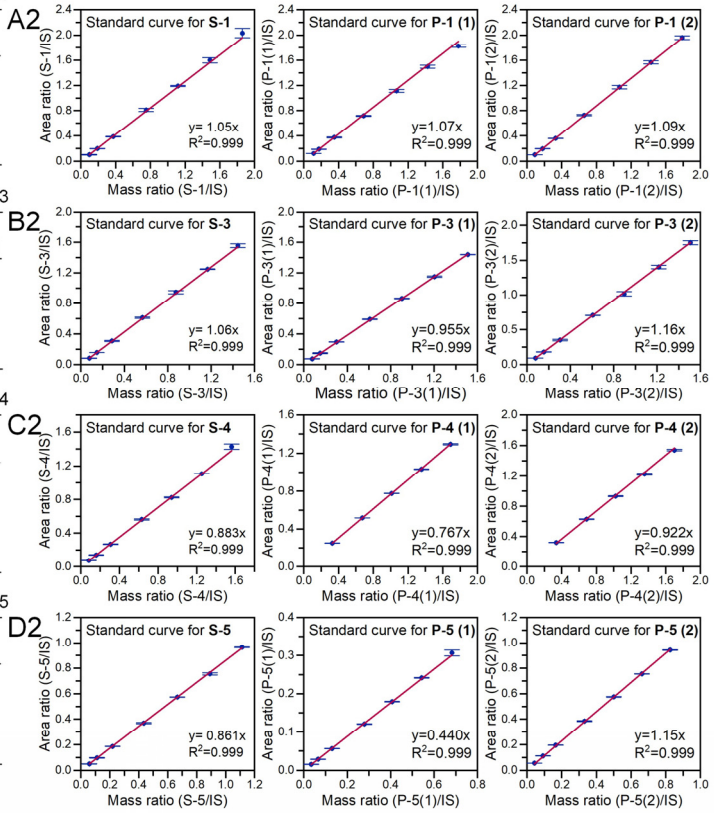

Fig. S8. GC analysis method. Temperature programs and standard curves for substrate S-1 and the corresponding products P-1 (A), substrate S-3 and the corresponding products P-3 (B), substrate S-4 and the corresponding products P-4 (C), substrate S-5 and the corresponding products P-5 (D).

7. Product yields of photocatalytic [2+2] cycloaddition reactions

General procedure:

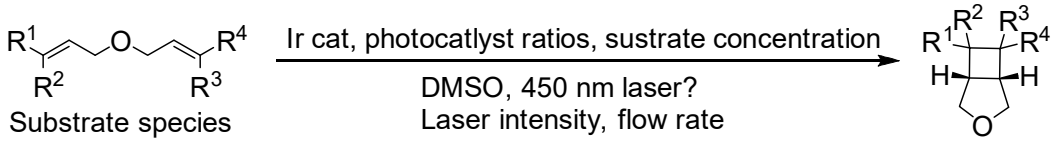

Unless otherwise noted, synthesis was performed in the LCW photocatalytic microreactor under the air at ambient temperature, with automatic control of the reaction temperature range in 25 ± 2 °C and irradiation from 450 nm lasers.

We measured the product yields of photocatalytic [2+2] cycloaddition reactions of 5 substrate species at a concentration of 0.01 M, which were catalyzed by 1 mol% of the photocatalyst Ir-1 with a residence time of 3.3 s in the LCW photocatalytic microreactor and a laser light intensity of 4.6 W.

The measurement results of the product yields of 6,7-diphenyl-3-oxabicyclo[3.2.0]heptane (**P-1**), 7-(furan-2-yl)-6,6-dimethyl-3-oxabicyclo[3.2.0]heptane (**P-2**), 1,6,6-trimethyl-7-phenyl-3-oxabicyclo[3.2.0]heptane (**P-3**), 7-(4-chlorophenyl)-6,6-dimethyl-3-oxabicyclo[3.2.0]heptane (**P-4**), and 7-(4-chlorophenyl)-6,6-dimethyl-3-oxabicyclo[3.2.0]heptane (**P-5**) are as follows.

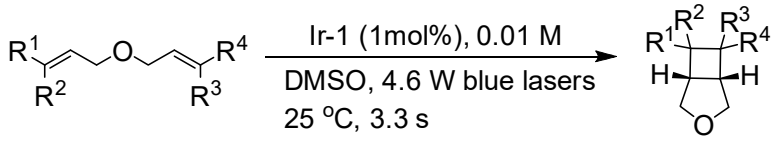

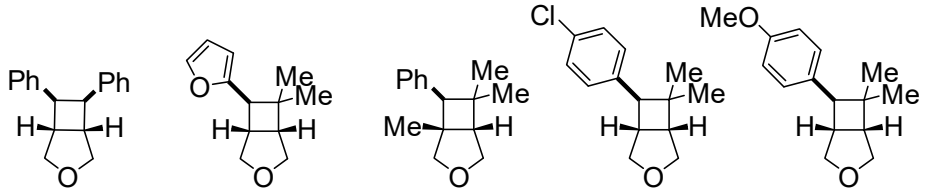

P-1 88% yield
3.7:1 *d.r.*

P-2 [b] 79% yield
7.8:1 *d.r.*

P-3 24% yield
1.5:1 *d.r.*

P-4 68% yield
>10:1 *d.r.*

P-5 69% yield
8.2:1 *d.r.*

[a] Reaction conditions: Substrate (1.0 equiv.) and Ir $(dFCF_3ppy)_2(dtbbpy)(PF_6)$ (Ir-1, 1 mol%) in DMSO (0.01 M) were performed in LCW photocatalytic microreactor under 4.6 W blue LEDs for 3.3 s (i.e., 200 磕/min). The yield of P-1, P-3, P-4 and P-5 was detected by GC, and 1-Nonanol was used as internal standard for P-1, P-3 and P-4, 1-Tetradecanol was used as internal standard for P-5. [b] The yield of P-2 was detected by NMR, and TMSPh was used as internal standard.

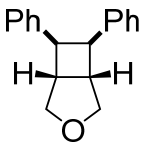

6,7-Diphenyl-3-oxabicyclo[3.2.0]heptane (P-1):

(1*R,5*S**,6*R**,7*S**) Diastereomer** (major): soild. ^{1}H NMR: (400 MHz, $CDCl_3$) δ 7.06 (dd, *J* = 7.2, 7.6 Hz, 4H), 6.98 (dd, *J* = 7.4, 7.4 Hz, 2H), 6.93 (d, *J* = 7.0 Hz, 4H), 4.10 (d, *J* = 9.6 Hz, 2H), 3.74 (d, *J* = 4.0 Hz, 2H), 3.73-3.66 (m, 2H), 3.34-3.25 (m, 2H); **(1*R**,5*S**,6*S**,7*S**) Diastereomer** (minor): Oil. ^{1}H NMR: (400 MHz, $CDCl_3$) δ 7.38-7.14 (m, 10H), 4.04 (d, *J* = 9.2 Hz, 1H), 3.88-3.76 (m, 2H), 3.67 (dd, *J* = 9.6, 6.8 Hz, 1H), 3.54 (dd, *J* = 9.2, 4.0 Hz, 1H), 3.48 (dd, *J* = 10.0, 7.2 Hz, 1H), 3.25 (dd, *J* = 15.8, 7.8 Hz, 1H), 3.16-3.06 (m, 1H). The analytical data were consistent with previously reported procedure[1].

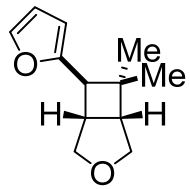

(1*R,5*R**,7*R**)-7-Furan-2-yl-6,6-dimethyl-3-oxa-bicyclo[3.2.0]heptane (P-2)**:

Diastereomer (major): oil. ^{1}H NMR: (400 MHz, $CDCl_3$) δ 7.35-7.31 (m, 1H), 6.34-6.28 (m, 1H), 6.03 (d, *J* = 3.0 Hz, 1H), 4.11 (d, *J* = 10.0 Hz, 1H), 3.80 (d, *J* = 9.2 Hz, 1H), 3.45 (dd, *J* = 10.0, 6.4 Hz, 1H), 3.42-3.37 (m, 1H), 3.19-3.12 (m, 1H), 2.86 (d, 1H), 2.40 (dd, *J* = 7.6, 7.2 Hz, 1H), 1.06 (s, 3H), 0.88 (s, 3H). The analytical data were consistent with previously reported procedure[1].

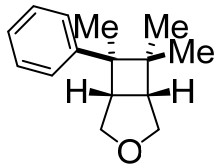

6,6,7-Trimethyl-7-phenyl-3-oxabicyclo[3.2.0]heptane (P-3):

(1*R,5*R**,7*R**)-Diastereomer** (major): oil. ^{1}H NMR: (400 MHz, $CDCl_3$) δ 7.37-7.26 (m, 4H), 7.24-7.17 (m, 1H), 6.51 (s, 1H), 5.45-5.36 (m, 1H), 4.02 (s, 2H), 3.99 (d, *J* = 7.6, 6.8 Hz, 2H), 1.91-1.88 (m, 3H), 1.77 (s, 3H), 1.69 (s, 3H). **(1*S**,5*R**,7*S**) Diastereomer** (minor): Oil. ^{1}H NMR: (400 MHz, $CDCl_3$) δ 7.31 (dd, *J* = 7.6, 7.2 Hz, 2H), 7.24-7.16 (m, 1H), 6.49 (s, 1H), 5.40-5.31 (m, 1H), 4.06 (s, 2H), 3.91 (d, *J* = 6.8 Hz, 2H), 1.97 (d, *J* = 1.4 Hz, 3H), 1.73 (s, 3H), 1.64 (s, 3H). The analytical data were consistent with previously reported procedure[1].

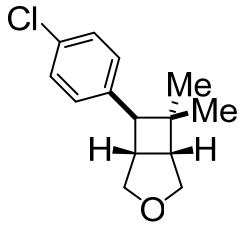

7-(4-Chlorophenyl)-6,6-dimethyl-3-oxabicyclo[3.2.0]heptane (P-4):

(1*R,5*R**,7*R**)-Diastereomer** (major): oil. ^{1}H NMR: (400 MHz, $CDCl_3$) δ 7.30-7.22 (m, 2H), 7.10-7.02 (m, 2H), 4.16 (d, *J* = 10.2 Hz, 1H), 3.77 (d, *J* = 9.2 Hz, 1H), 3.50 (dd, *J* = 10.2, 6.8 Hz, 1H), 3.43 (dd, *J* = 9.0, 4.4 Hz, 1H), 3.25-3.17 (m, 1H), 2.95 (d, *J* = 7.2 Hz, 1H), 2.40 (dd, *J* = 7.6, 7.4 Hz, 1H), 1.09 (s, 3H), 0.73 (s, 3H). **(1*S**,5*R**,7*S**) Diastereomer** (minor): Oil. ^{1}H NMR: (400 MHz, $CDCl_3$) δ 7.26-7.20 (m, 4H), 4.16 (d, *J* = 9.6 Hz, 1H), 4.09 (d, *J* = 10.2 Hz, 1H), 3.47 (dd, *J* = 10.0, 5.8 Hz, 1H), 3.41 (dd, *J* = 10.0, 6.4 Hz, 1H), 3.31 (d, *J* = 9.6 Hz, 1H), 3.26-3.17 (m, 1H), 2.62 (dd, *J* = 7.6, 6.4 Hz, 1H), 1.28 (s, 3H), 0.86 (s, 3H). The analytical data were consistent with previously reported procedure[1].

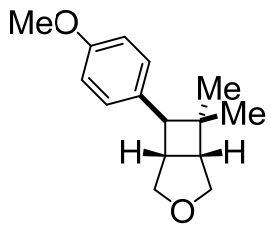

7-(4-Methoxyphenyl)-6,6-dimethyl-3-oxabicyclo[3.2.0]heptane (P-5):

(1*R,5*R**,7*R**)-Diastereomer** (major): oil. ^{1}H NMR: (400 MHz, $CDCl_3$) δ 7.06 (d, *J* = 8.4 Hz, 2H), 6.88-6.82 (m, 2H), 4.15 (d, *J* = 10.0 Hz, 1H), 3.82-3.73 (m, 4H), 3.50 (dd, *J* = 9.8, 6.8 Hz, 1H), 3.42 (dd, *J* = 8.8, 4.4 Hz, 1H), 3.25-3.15 (m, 1H), 2.91 (d, *J* = 7.6 Hz, 1H), 2.38 (dd, *J* = 7.6, 7.2 Hz, 1H), 1.08 (s, 3H), 0.73 (s, 3H). **(1*S**,5*R**,7*S**) Diastereomer** (minor): Oil. ^{1}H NMR: (400 MHz, $CDCl_3$) δ 7.25-7.19 (m, 2H), 6.86-6.80 (m, 2H), 4.15 (dd, *J* = 9.8, 6.8 Hz, 2H), 3.79 (s, 3H), 3.47 (dd, *J* = 9.8, 5.6 Hz, 1H), 3.40 (dd, *J* = 10.0, 6.4 Hz, 1H), 3.30 (d, *J* = 9.8 Hz, 1H), 3.25-3.16 (m, 1H), 2.60 (dd, *J* = 7.6, 5.8 Hz, 1H), 1.26 (s, 3H), 0.87 (s, 3H). The analytical data were consistent with previously reported procedure[1].

For further validation of the robotic system, we measured the product yields under representative conditions of photocatalytic [2+2] cycloaddition reaction from the 5 substrate species (i.e., 145 conditions of S-1, and 13 conditions per substrate species of S-2, S-3, S-4 and S-5). Using the robotic system, 145 representative screening conditions of S-1 were selected to perform the photocatalytic

[2+2] cycloaddition reaction and their product yields were analyzed with the GC method, involving all 5 variables (i.e., laser light intensity, substrate concentration, flow rate, photocatalyst species and photocatalyst ratios) of the screening in Table S3. As the results of the 5 photocatalyst species (i.e., Ir-1, Ir-2, Ir-3, Ir-4 and Ir-5), the synthesis using Ir-1 as a photocatalyst could obtain the highest product yields of P-1 in 92%. The results on different flow rates and laser light intensities of S-2, S-3, S-4 and S-5 systems are listed in Table S4, S5, S6 and S7, giving P-2 in 7-79% yields, P-3 in 2-24% yields, P-4 in 10-68% yields, and P-5 in 7-69% yields, respectively. With the flow rate of 200 μL/min (i.e., 3.3 s residence time) and laser light intensity of 4.6 W, the reaction could produce P-2 in 79% yield, P-3 in 24% yield, P-4 in 68% yield and P-5 in 69% yield.

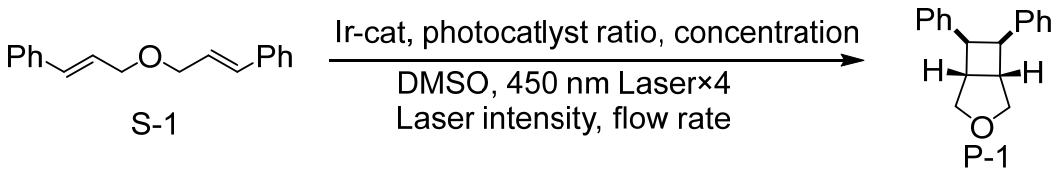

Table S3. Product yields of 145 representative conditions of S-1 system

Entry	PC species	Flow rate (μL/min)	Concentration (M)	PC ratio (mol%)	Light intensity (W)	Yield (%)	d.r.	Recovery (%)
1	Ir-1	200	0.005	0.5	-	-	-	98
2	Ir-1	200	0.005	0.5	0.8	8	3.9:1	89
3	Ir-1	200	0.005	0.5	1.5	26	3.8:1	65
4	Ir-1	200	0.005	0.5	2.3	43	3.8:1	45
5	Ir-1	200	0.005	0.5	3.1	57	3.6:1	29
6	Ir-1	200	0.005	0.5	3.9	66	3.6:1	19
7	Ir-1	200	0.005	0.5	4.6	72	3.7:1	14
8	Ir-1	200	0.005	1.0	0.8	20	3.7:1	72
9	Ir-1	200	0.005	1.0	1.5	53	3.7:1	35
10	Ir-1	200	0.005	1.0	2.3	70	3.8:1	15
11	Ir-1	200	0.005	1.0	3.1	80	3.8:1	7

Entry	PC species	Flow rate (μL/min)	Concentration (M)	PC ratio (mol%)	Light intensity (W)	Yield (%)	d.r.	Recovery (%)
12	Ir-1	200	0.005	1.0	3.9	84	3.7:1	3
13	Ir-1	200	0.005	1.0	4.6	87	3.7:1	/
14	Ir-1	200	0.005	1.5	0.8	31	3.6:1	55
15	Ir-1	200	0.005	1.5	1.5	61	3.6:1	22
16	Ir-1	200	0.005	1.5	2.3	77	3.8:1	8
17	Ir-1	200	0.005	1.5	3.1	84	3.7:1	3
18	Ir-1	200	0.005	1.5	3.9	86	3.7:1	/
19	Ir-1	200	0.005	1.5	4.6	86	3.7:1	/
20	Ir-1	200	0.005	2.0	0.8	41	3.7:1	47
21	Ir-1	200	0.005	2.0	1.5	71	3.7:1	15
22	Ir-1	200	0.005	2.0	2.3	83	3.7:1	5
23	Ir-1	200	0.005	2.0	3.1	85	3.6:1	2
24	Ir-1	200	0.005	2.0	3.9	87	3.6:1	/
25	Ir-1	200	0.005	2.0	4.6	89	3.7:1	/
26	Ir-1	200	0.01	0.5	0.8	24	3.8:1	66
27	Ir-1	200	0.01	0.5	1.5	46	3.8:1	40
28	Ir-1	200	0.01	0.5	2.3	61	3.7:1	25
29	Ir-1	200	0.01	0.5	3.1	70	3.7:1	16
30	Ir-1	200	0.01	0.5	3.9	76	3.8:1	10
31	Ir-1	200	0.01	0.5	4.6	80	3.7:1	7
32	Ir-1	200	0.01	1.0	0.8	30	3.7:1	62
33	Ir-1	200	0.01	1.0	1.5	59	3.8:1	28
34	Ir-1	200	0.01	1.0	2.3	76	3.8:1	12
35	Ir-1	200	0.01	1.0	3.1	84	3.8:1	4
36	Ir-1	200	0.01	1.0	3.9	86	3.7:1	2
37	Ir-1	200	0.01	1.0	4.6	88	3.7:1	/
38	Ir-1	200	0.01	1.5	0.8	44	3.7:1	45
39	Ir-1	200	0.01	1.5	1.5	74	3.7:1	13
40	Ir-1	200	0.01	1.5	2.3	85	3.6:1	3
41	Ir-1	200	0.01	1.5	3.1	90	3.7:1	/
42	Ir-1	200	0.01	1.5	3.9	90	3.7:1	/
43	Ir-1	200	0.01	1.5	4.6	91	3.7:1	/

Entry	PC species	Flow rate (μL/min)	Concentration (M)	PC ratio (mol%)	Light intensity (W)	Yield (%)	d.r.	Recovery (%)
44	Ir-1	200	0.01	2.0	0.8	47	3.5:1	38
45	Ir-1	200	0.01	2.0	1.5	81	3.7:1	8
46	Ir-1	200	0.01	2.0	2.3	88	3.7:1	/
47	Ir-1	200	0.01	2.0	3.1	90	3.7:1	/
48	Ir-1	200	0.01	2.0	3.9	88	3.6:1	/
49	Ir-1	200	0.01	2.0	4.6	89	3.6:1	/
50	Ir-1	200	0.015	0.5	0.8	12	3.6:1	84
51	Ir-1	200	0.015	0.5	1.5	29	3.8:1	64
52	Ir-1	200	0.015	0.5	2.3	44	3.8:1	45
53	Ir-1	200	0.015	0.5	3.1	59	3.7:1	28
54	Ir-1	200	0.015	0.5	3.9	70	3.8:1	18
55	Ir-1	200	0.015	0.5	4.6	77	3.8:1	11
56	Ir-1	200	0.015	1.0	0.8	15	3.7:1	81
57	Ir-1	200	0.015	1.0	1.5	40	3.8:1	48
58	Ir-1	200	0.015	1.0	2.3	58	3.8:1	29
59	Ir-1	200	0.015	1.0	3.1	75	3.7:1	12
60	Ir-1	200	0.015	1.0	3.9	83	3.7:1	6
61	Ir-1	200	0.015	1.0	4.6	86	3.8:1	3
62	Ir-1	200	0.015	1.5	0.8	18	3.6:1	77
63	Ir-1	200	0.015	1.5	1.5	52	3.8:1	37
64	Ir-1	200	0.015	1.5	2.3	71	3.8:1	16
65	Ir-1	200	0.015	1.5	3.1	85	3.7:1	5
66	Ir-1	200	0.015	1.5	3.9	89	3.7:1	-
67	Ir-1	200	0.015	1.5	4.6	90	3.7:1	-
68	Ir-1	200	0.015	2.0	0.8	24	3.6:1	69
69	Ir-1	200	0.015	2.0	1.5	59	3.8:1	29
70	Ir-1	200	0.015	2.0	2.3	78	3.7:1	10
71	Ir-1	200	0.015	2.0	3.1	89	3.7:1	2
72	Ir-1	200	0.015	2.0	3.9	91	3.7:1	-
73	Ir-1	200	0.015	2.0	4.6	91	3.7:1	-
74	Ir-1	200	0.02	0.5	0.8	9	3.5:1	89
75	Ir-1	200	0.02	0.5	1.5	21	3.6:1	73

Entry	PC species	Flow rate (μL/min)	Concentration (M)	PC ratio (mol%)	Light intensity (W)	Yield (%)	d.r.	Recovery (%)
76	Ir-1	200	0.02	0.5	2.3	34	3.7:1	56
77	Ir-1	200	0.02	0.5	3.1	49	3.8:1	39
78	Ir-1	200	0.02	0.5	3.9	61	3.8:1	26
79	Ir-1	200	0.02	0.5	4.6	69	3.8:1	18
80	Ir-1	200	0.02	1.0	0.8	18	3.6:1	76
81	Ir-1	200	0.02	1.0	1.5	36	3.7:1	53
82	Ir-1	200	0.02	1.0	2.3	56	3.8:1	30
83	Ir-1	200	0.02	1.0	3.1	74	3.7:1	14
84	Ir-1	200	0.02	1.0	3.9	82	3.7:1	7
85	Ir-1	200	0.02	1.0	4.6	86	3.7:1	4
86	Ir-1	200	0.02	1.5	0.8	25	3.6:1	69
87	Ir-1	200	0.02	1.5	1.5	47	3.6:1	43
88	Ir-1	200	0.02	1.5	2.3	69	3.8:1	20
89	Ir-1	200	0.02	1.5	3.1	83	3.7:1	7
90	Ir-1	200	0.02	1.5	3.9	88	3.7:1	3
91	Ir-1	200	0.02	1.5	4.6	90	3.7:1	-
92	Ir-1	200	0.02	2.0	0.8	31	3.6:1	60
93	Ir-1	200	0.02	2.0	1.5	58	3.7:1	30
94	Ir-1	200	0.02	2.0	2.3	78	3.7:1	10
95	Ir-1	200	0.02	2.0	3.1	89	3.7:1	3
96	Ir-1	200	0.02	2.0	3.9	92	3.7:1	-
97	Ir-1	200	0.02	2.0	4.6	91	3.7:1	-
98	Ir-1	600	0.01	1.0	0.8	3	3.9:1	93
99	Ir-1	600	0.01	1.0	1.5	10	3.6:1	83
100	Ir-1	600	0.01	1.0	2.3	21	3.7:1	68
101	Ir-1	600	0.01	1.0	3.1	31	3.8:1	55
102	Ir-1	600	0.01	1.0	3.9	42	3.8:1	44
103	Ir-1	600	0.01	1.0	4.6	48	3.8:1	36
104	Ir-1	500	0.01	1.0	0.8	2	-	93
105	Ir-1	500	0.01	1.0	1.5	11	3.6:1	81
106	Ir-1	500	0.01	1.0	2.3	24	3.6:1	63
107	Ir-1	500	0.01	1.0	3.1	35	3.8:1	51

Entry	PC species	Flow rate (μL/min)	Concentration (M)	PC ratio (mol%)	Light intensity (W)	Yield (%)	d.r.	Recovery (%)
108	Ir-1	500	0.01	1.0	3.9	45	3.8:1	39
109	Ir-1	500	0.01	1.0	4.6	53	3.8:1	30
110	Ir-1	400	0.01	1.0	0.8	4	3.9:1	92
111	Ir-1	400	0.01	1.0	1.5	13	3.5:1	77
112	Ir-1	400	0.01	1.0	2.3	30	3.8:1	57
113	Ir-1	400	0.01	1.0	3.1	43	3.7:1	42
114	Ir-1	400	0.01	1.0	3.9	54	3.7:1	31
115	Ir-1	400	0.01	1.0	4.6	61	3.7:1	23
116	Ir-1	300	0.01	1.0	0.8	5	3.3:1	89
117	Ir-1	300	0.01	1.0	1.5	17	3.6:1	73
118	Ir-1	300	0.01	1.0	2.3	38	3.6:1	48
119	Ir-1	300	0.01	1.0	3.1	54	3.7:1	31
120	Ir-1	300	0.01	1.0	3.9	62	3.8:1	21
121	Ir-1	300	0.01	1.0	4.6	69	3.8:1	14
122	Ir-2	200	0.01	1.0	0.8	6	3.9:1	93
123	Ir-2	200	0.01	1.0	1.5	16	3.6:1	80
124	Ir-2	200	0.01	1.0	2.3	30	3.8:1	62
125	Ir-2	200	0.01	1.0	3.1	45	3.7:1	46
126	Ir-2	200	0.01	1.0	3.9	55	3.7:1	34
127	Ir-2	200	0.01	1.0	4.6	63	3.8:1	27
128	Ir-3	200	0.01	1.0	0.8	10	3.6:1	89
129	Ir-3	200	0.01	1.0	1.5	28	3.8:1	65
130	Ir-3	200	0.01	1.0	2.3	46	3.8:1	44
131	Ir-3	200	0.01	1.0	3.1	56	3.8:1	32
132	Ir-3	200	0.01	1.0	3.9	63	3.8:1	25
133	Ir-3	200	0.01	1.0	4.6	67	3.8:1	21
134	Ir-4	200	0.01	1.0	0.8	4	3.9:1	97
135	Ir-4	200	0.01	1.0	1.5	14	3.6:1	83
136	Ir-4	200	0.01	1.0	2.3	24	3.7:1	70
137	Ir-4	200	0.01	1.0	3.1	31	3.7:1	62
138	Ir-4	200	0.01	1.0	3.9	36	3.6:1	56
139	Ir-4	200	0.01	1.0	4.6	40	3.7:1	51

Entry	PC species	Flow rate (μL/min)	Concentration (M)	PC ratio (mol%)	Light intensity (W)	Yield (%)	d.r.	Recovery (%)
140	Ir-5	200	0.01	1.0	0.8	5	3.7:1	95
141	Ir-5	200	0.01	1.0	1.5	17	3.7:1	80
142	Ir-5	200	0.01	1.0	2.3	32	3.7:1	62
143	Ir-5	200	0.01	1.0	3.1	46	3.7:1	48
144	Ir-5	200	0.01	1.0	3.9	55	3.7:1	36
145	Ir-5	200	0.01	1.0	4.6	62	3.7:1	29

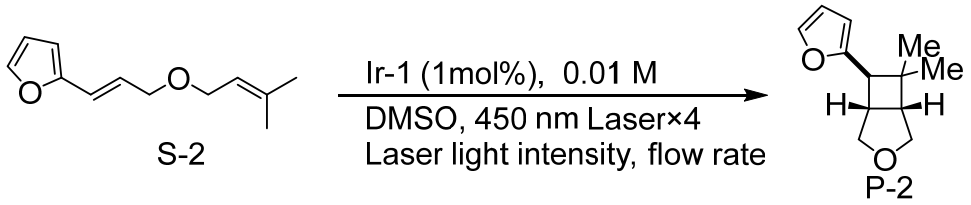

Table S4. Product yields of 13 representative conditions of S-2

Entry	Flow rate (μL/min)	Light intensity (W)	Yield (%)	d.r.	Recovery (%)
1	600	0.8	7	6.0:1	80
2	600	1.5	11	5.0:1	70
3	600	2.3	19	8.5:1	60
4	600	3.1	26	7.7:1	53
5	600	3.9	32	7.0:1	47
6	600	4.6	40	7.0:1	40
7	200	0.8	10	9.0:1	73
8	200	1.5	25	7.3:1	54
9	200	2.3	44	7.8:1	36
10	200	3.1	59	7.4:1	22
11	200	3.9	68	8.7:1	10
12	200	4.6	79	7.8:1	5
13	200	-	-	-	87

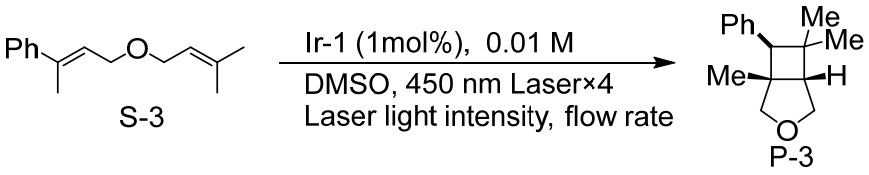

Table S5. Product yields of 13 representative conditions of S-3

Entry	Flow rate (μL/min)	Light intensity (W)	Yield (%)	d.r.	Recovery (%)
1	600	0.8	2	2.0:1	82
2	600	1.5	3	1.6:1	68
3	600	2.3	6	2.0:1	58
4	600	3.1	7	1.8:1	54
5	600	3.9	8	1.7:1	48
6	600	4.6	9	1.5:1	47
7	200	0.8	4	1.6:1	58
8	200	1.5	9	1.7:1	46
9	200	2.3	13	1.6:1	42
10	200	3.1	17	1.6:1	40
11	200	3.9	21	1.5:1	38
12	200	4.6	24	1.5:1	37
13	200	-	-	-	106

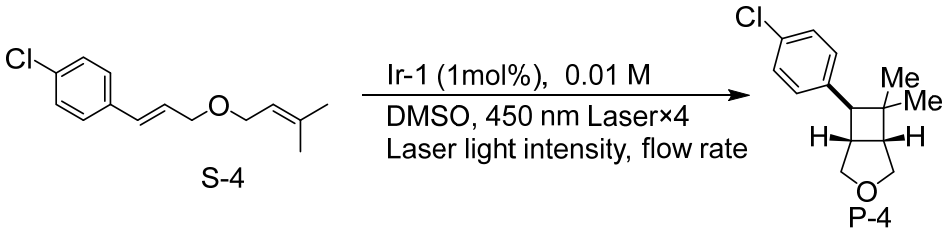

Table S6. Product yields of 13 representative conditions of S-4

Entry	Flow rate (μL/min)	Light intensity (W)	Yield (%)	d.r.	Recovery (%)
1	600	0.8	10	＞10:1	74
2	600	1.5	18	＞10:1	60
3	600	2.3	23	＞10:1	51
4	600	3.1	27	＞10:1	44
5	600	3.9	30	＞10:1	39
6	600	4.6	36	＞10:1	35
7	200	0.8	19	＞10:1	51
8	200	1.5	34	＞10:1	36
9	200	2.3	45	＞10:1	27
10	200	3.1	54	＞10:1	19
11	200	3.9	61	＞10:1	15
12	200	4.6	68	＞10:1	11
13	200	-	-	-	104

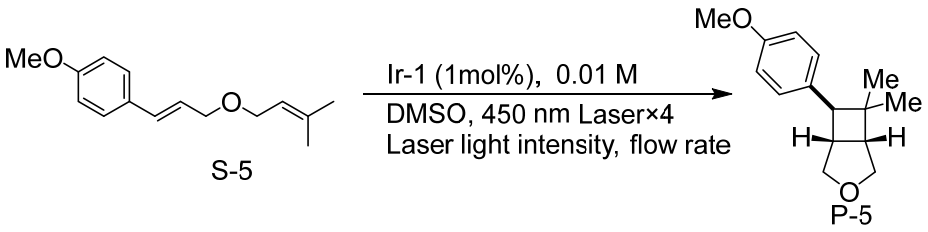

Table S7. Product yields of 13 representative conditions of S-5

Entry	Flow rate (μL/min)	Light intensity (W)	Yield (%)	d.r.	Recovery (%)
1	600	0.8	7	8.2:1	76
2	600	1.5	14	8.4:1	62
3	600	2.3	20	7.9:1	50
4	600	3.1	27	8.5:1	42
5	600	3.9	32	8.2:1	35
6	600	4.6	37	8.0:1	30
7	200	0.8	19	8.1:1	50
8	200	1.5	36	8.0:1	30
9	200	2.3	49	8.1:1	18
10	200	3.1	63	7.6:1	11
11	200	3.9	71	7.2:1	6
12	200	4.6	69	8.2:1	3
13	200	-	-	-	99

8. Relationship between steady-state absorbance and product yield

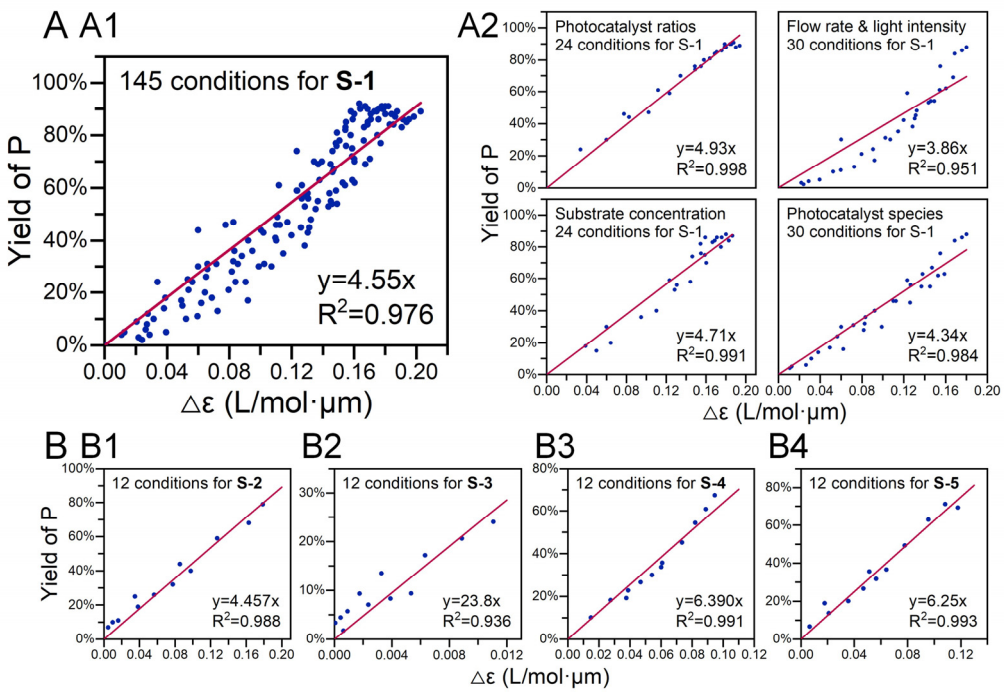

Fig. S9. Relationship between steady-state absorbance data and product yields. (A) Relationship between 145 representative steady-state absorbance data and product yields of substrate S-1 with R^2 = 0.976 (A1), including different variables such as photocatalyst ratios, flow rates, laser light intensities, substrate concentrations and photocatalyst species (A2). (B) Relationships between 12 representative steady-state absorbance data for substrates S-2 (B1), S-3 (B2), S-4 (B3) and S-5 (B4), respectively, with the R^2 value range of 0.936-0.993.

After obtaining product yields for representative conditions by GC and NMR methods, we determined the relationship between the steady-state absorbance data and product yields by linear fitting. To calibrate the effect of different concentrations of the reaction mixture, we first converted all the selected 145 steady-state absorbance data of S-1 into the value of change in molar absorbance coefficient (Δε), and the linear fitting showed a quite good correlation (R^2 = 0.976, n = 145) between

the Δε values and product yields (Fig. S9A). In addition, the linear fitting was also attempted with some representative data from other substrate species (i.e., 12 data per substrate species for S-2, S-3, S-4 and S-5 systems, respectively), and similar results were obtained with the R^2 value range of 0.936-0.993 (Fig. S9B). These results demonstrated the feasibility and reliability of using the online UV-Vis absorption spectroscopy method to monitor the progress of the photocatalytic [2+2] cycloaddition reaction and to evaluate the product yields. All the steady-state absorbance data obtained were then converted into product yields for further data analysis.

9. Performance comparison between the batch and flow synthesis systems

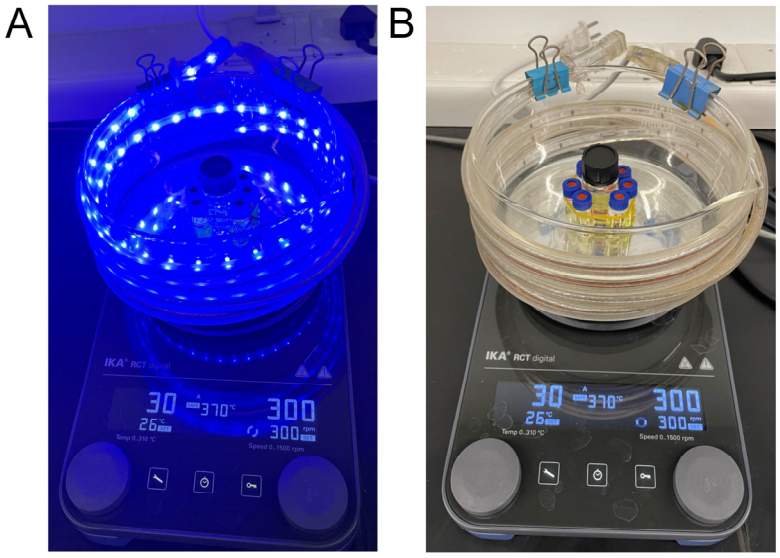

Fig. S10. Setup for batch synthesis of different substrate concentrations. Batch synthesis performed under stirring and light irradiation (A), with standard 2-mL vials as the reactors symmetrically placed in the center of the coiled LED (B).

The present LCW photocatalytic microreactor showed the potential to achieve rapid photocatalytic synthesis with high product yields at higher substrate concentration ranges, so we

screened the conditions of substrate S-1 with photocatalyst Ir-1 (1 mol%) using the LCW photocatalytic microreactor-based system and a batch photocatalytic reactor at different concentrations from 0.01 M to 2.0 M, respectively. Flow synthesis at different concentrations were carried out with the LCW photocatalytic microreactor using the procedure as previously described. As for the batch mode, standard 2 mL glass vials were used as the reactors, and the reaction mixture was stirred and irradiated by a 10 W (5 W/m * 2 m) 450 nm coiled LED for 4 h (Fig. S10A). In order to ensure that all vials could be uniformly illuminated and the synthesis was performed at ambient temperature, the vials were symmetrically placed in the center of the coiled LED strip (Fig. S10B).

10. Hyperparameters of the AI models

In the AI-assisted absorbance prediction, the performance of each AI model usually related to several to even a dozen of hyperparameters, from which 1-6 hyperparameters with large impacts on model performance were empirically selected and optimized using the Grid Search method (i.e., the GridSearchCV in sklearn.model_selection). Based on the default values of each hyperparameter, the single training time consumed by the model, the characteristics of the dataset (i.e., amount of data and number of features), and prior experience, the selection ranges of these hyperparameters to be searched (i.e., the param_grid parameter in GridSearchCV) were generated in advance, and the AI models with different hyperparameter values were trained, evaluated, and optimized with 5-fold cross-validation. The optimal hyperparameter values were obtained from GridSearchCV's best_params_, and the optimal model was obtained from GridSearchCV's best_estimator_. For example, for the Random Forest regression model, the selected hyperparameters and their values included: param_grid = {'n_estimators': [250, 350, 500], 'max_depth':[10, 30, 50], 'max_features': [4, 6]}. The optimal hyperparameters and their values included: {'max_depth': 30, 'max_features': 6,

'n_estimators': 350}. Considering that each AI model involved different hyperparameters, each of the 10 AI models was analyzed specifically to obtain the optimal hyperparameter values, respectively (Table S8). The linear regression model was not optimized for hyperparameters as sklearn does not have hyperparameters set for it.

Table S8. Selected hyperparameters and their values of the 10 AI models, with the optimal hyperparameter values.

Regression models	Selected hyperparameters and values	Optimal hyperparameter values by grid search
PLSR	{'n_components': [1, 2, 5, 9]}	{'n_components': 9}
Linear	No model parameters need to screen	-
Adaboosting	{'n_estimators': [50, 100, 200], 'learning_rate':[0.1, 0.5, 1]}	{'learning_rate': 0.1, 'n_estimators': 100}
ExtraTree	{'max_depth': [3, 10, 20], 'min_samples_leaf':[5, 10, 20], 'min_samples_split':[10, 30, 50]}	{'max_depth': 20, 'min_samples_leaf': 5, 'min_samples_split': 10}
SVR	{'C': [0.1, 1, 5, 10]}	{'C': 1}
KNN	{'weights':['distance'], 'n_neighbors': [5, 10, 30], 'p':[1, 2, 4]}	{'n_neighbors': 5, 'p': 1, 'weights': 'distance'}
MLP	{'solver':['lbfgs'], 'activation':['relu'], 'learning_rate_init':[0.001], 'hidden_layer_sizes':[(50,50), (50,20), (50,50,20)], 'max_iter': [100, 200], 'alpha':[0.001, 0.01]}	{'activation': 'relu', 'alpha': 0.001, 'hidden_layer_sizes': (50, 50, 20), 'learning_rate_init': 0.001, 'max_iter': 200, 'solver': 'lbfgs'}
Random Forest	{'n_estimators': [250, 350, 500], 'max_depth':[10, 30, 50], 'max_features': [4, 6]}	{'max_depth': 30, 'max_features': 6, 'n_estimators': 350}
Cascade Forest	{'max_layers': [20, 30], 'n_estimators':[2, 10], 'n_trees':[100, 150]}	{'max_layers': 20, 'n_estimators': 2, 'n_trees': 150}
XGB	{'n_estimators': [200, 300, 500]}	{'n_estimators': 500}

In the AI-assisted cross-species prediction, we used the XGBoost's default hyperparameters because they could offer good performance.

11 Cross-validation studies

11.1 Cross-validation study of AI-assisted absorbance prediction

Table S9. The 10-fold cross-validation study performed on the entire dataset in the AI-assisted absorbance prediction. The model performance metrics include the MAE, RMSE, and R^2 values and their means, standard deviations, and coefficients of variation (CV).

Entry	Train Index	Test Index	Metrics of the test set		
			MAE	RMSE	R^2
1	[0 1 2 ... 1197 1198 1199]	[1200 1201 1202 ... 11997 11998 11999]	0.0182	0.0289	0.961
2	[1200 1201 1202 ... 2397 2398 2399]	[0 1 2 ... 1198 1199 2400... 11997 11998 11999]	0.0188	0.0296	0.959
3	[2400 2401 2402 ... 3597 3598 3599]	[0 1 2 ... 2398 2399 3600... 11997 11998 11999]	0.0188	0.0304	0.956
4	[3600 3601 3602 ... 4797 4798 4799]	[0 1 2 ... 3598 3599 4800... 11997 11998 11999]	0.0179	0.0292	0.960
5	[4800 4801 4802 ... 5997 5998 5999]	[0 1 2 ... 4798 4799 6000... 11997 11998 11999]	0.0191	0.0309	0.955
6	[6000 6001 6002 ... 7197 7198 7199]	[0 1 2 ... 5998 5999 7200... 11997 11998 11999]	0.0180	0.0286	0.962
7	[7200 7201 7202 ... 8397 8398 8399]	[0 1 2 ... 7198 7199 8400... 11997 11998 11999]	0.0177	0.0277	0.964
8	[8400 8401 8402 ... 9597 9598 9599]	[0 1 2 ... 8398 8399 9600... 11997 11998 11999]	0.0203	0.0327	0.950
9	[9600 9601 9602 ... 10797 10798 10799]	[0 1 2 ... 9598 9599 10800... 11997 11998 11999]	0.0199	0.0325	0.951
10	[10800 10801 10802 ... 11997 11998 11999]	[0 1 2 ... 10797 10798 10799]	0.0184	0.0299	0.958
Mean			0.0187	0.0300	0.958
Standard deviation			0.000842	0.00164	0.00469
Coefficient of variation (CV)			4.50%	5.44%	0.49%

In the task of predicting 12,000 steady-state absorbance data using 10% of the non-steady-state absorbance data as the training set of the XGB model, a 10-fold cross-validation study was performed on the entire dataset by dividing the dataset equally into 10 parts (i.e., 0-10%, 10-20%, ..., 90-100%). Each time, one part of them was taken as the training set and the remaining 9 parts as the test set, resulting in a total of 10 kinds of training/test sets. To ensure the randomness in the extracting of the

training sets, the data in the dataset were disrupted in order before performing the 10-fold cross-validation. The optimized XGB regression model (i.e., n_estimators hyperparameter taking the value of 500 filtered by grid search) was trained and evaluated using the 10 training/test sets, and the model performance metrics including the MAE, RMSE, and R^2 values and their means, standard deviations, and coefficients of variation (CV) were calculated (Table S9). The results showed that the model performance metrics obtained from the dataset as shown in Figure 4A had no significant difference, and the coefficients of variation were 4.50% for MAE, 5.44% for RSME and 0.49% for R^2, respectively, indicating the good generalization ability of the model.

11.2 Cross-validation studies of AI-assisted cross-species prediction

In the cross-species prediction, the cross-validation studies were performed for both cross-photocatalyst and cross-substrate prediction. In the cross-photocatalyst prediction, the data of 4 photocatalyst species were used as the training set to predict the yields of the other 1 photocatalyst species, and the data of 3 photocatalyst species were used as the training set to predict the yields of the other 2 photocatalyst species, with box plots showing the product yield results (Fig. S11A).

In the cross-substrate prediction, the data of 3 substrate species were used as the training set to predict the yields of the other 1 substrate species, and the data of 2 substrate species were used as the training set to predict the yields of the other 2 substrate species, with box plots showing the product yield results (Fig. S11B). For instance, we used the data of S-1, S-2, and S-4 as the training set to predict the yields of S-5, achieving MAE=0.0698 and RMSE=0.0878 (Fig. S11B1). The distinct effects of the 5 photocatalyst species on S-5 were accurately predicted with Ir-1 as the optimal photocatalyst. With a smaller training set of S-1 and S-2, the prediction for S-4 and S-5 were also completed with MAE=0.0772 and RMSE=0.0999 (Fig. S11B2).

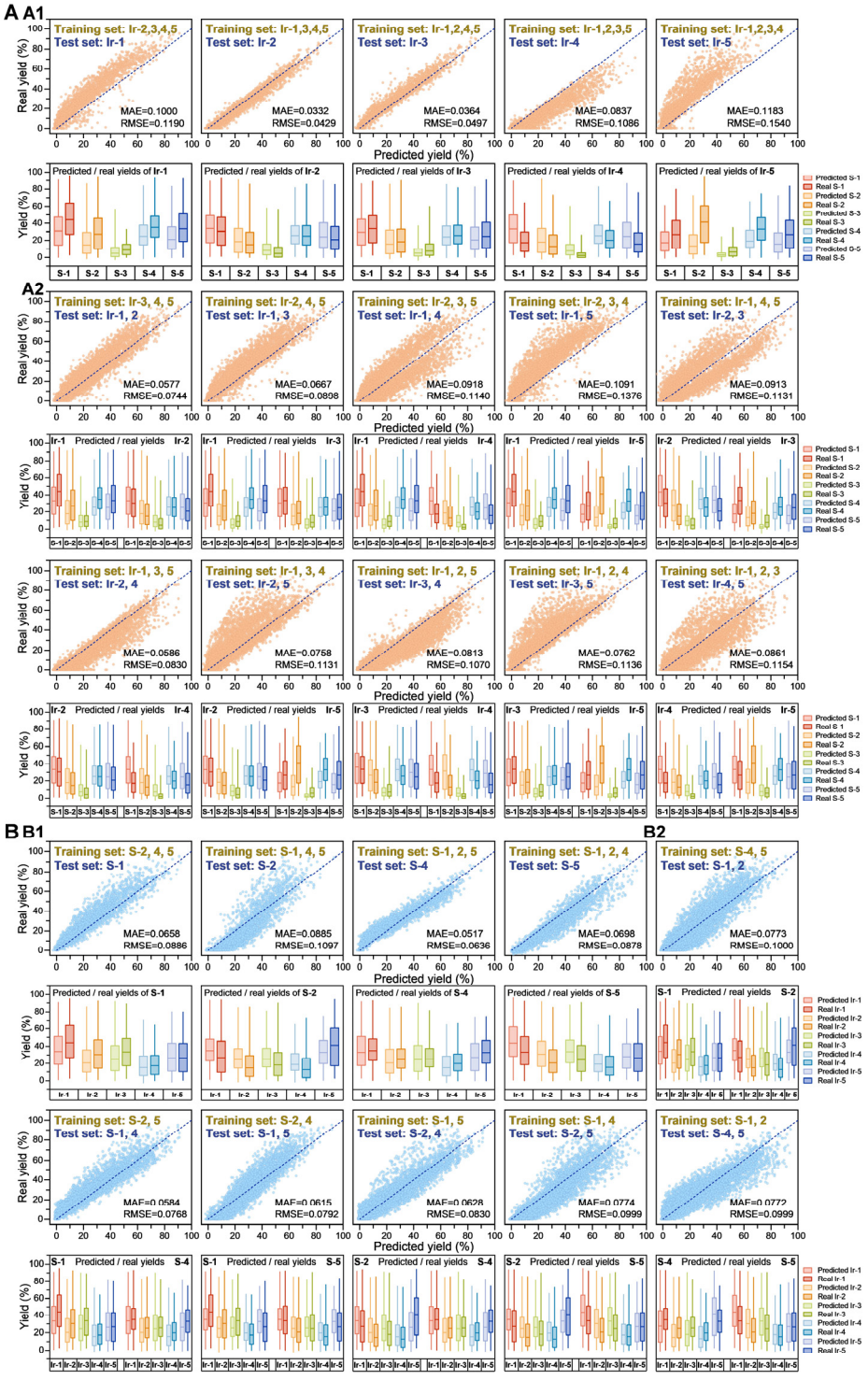

Fig. S11. The cross-validation studies for the cross-species prediction. The results of the cross-validation studies including the cross-photocatalyst (A) and the cross-substrate prediction (B).

The performance parameters of the test set for all possible cases were obtained in the cross-validation studies, and their small errors demonstrated the stability of the method (Table S10, S11).

Table S10. Model performance metrics include MAE and RMSE values, with their means and standard deviations, obtained in cross-validation studies for the cross-photocatalyst prediction.

Entry	Train set	Test set	Metrics of the test set	
			MAE	RMSE
1	Ir-2,3,4,5	Ir-1	0.1000	0.1190
2	Ir-1,3,4,5	Ir-2	0.0332	0.0429
3	Ir-1,2,4,5	Ir-3	0.0364	0.0497
4	Ir-1,2,3,5	Ir-4	0.0837	0.1086
5	Ir-1,2,3,4	Ir-5	0.1183	0.1540
	Mean		0.0743	0.0958
	Standard deviation		0.0341	0.0424
1	Ir-3,4,5	Ir-1,2	0.0577	0.0774
2	Ir-2,4,5	Ir-1,3	0.0667	0.0898
3	Ir-2,3,5	Ir-1,4	0.0918	0.1140
4	Ir-2,3,4	Ir-1,5	0.1091	0.1376
5	Ir-1,4,5	Ir-2,3	0.0913	0.1131
6	Ir-1,3,5	Ir-2,4	0.0586	0.0830
7	Ir-1,3,4	Ir-2,5	0.0758	0.1131
8	Ir-1,2,5	Ir-3,4	0.0813	0.1070
9	Ir-1,2,4	Ir-3,5	0.0762	0.1136
10	Ir-1,2,3	Ir-4,5	0.0861	0.1154
	Mean		0.0795	0.1064
	Standard deviation		0.0152	0.0171

Table S11. Model performance metrics include MAE and RMSE values, with their means and standard deviations, obtained in cross-validation studies for the cross-substrate prediction.

Entry	Train set	Test set	Metrics of the test set	
			MAE	RMSE
1	S-2,4,5	S-1	0.0658	0.0886
2	S-1,4,5	S-2	0.0885	0.1097
3	S-1,2,5	S-4	0.0517	0.0636
4	S-1,2,4	S-5	0.0698	0.0878
	Mean		0.0690	0.0874
	Standard deviation		0.0131	0.0164
1	S-4,5	S-1,2	0.0773	0.1000
2	S-2,5	S-1,4	0.0584	0.0768
3	S-2,4	S-1,5	0.0615	0.0792
4	S-1,5	S-2,4	0.0628	0.0830
5	S-1,4	S-2,5	0.0774	0.0999
6	S-1,2	S-4,5	0.0772	0.0999
	Mean		0.0691	0.0898
	Standard deviation		0.00831	0.0103

12. NMR spectra

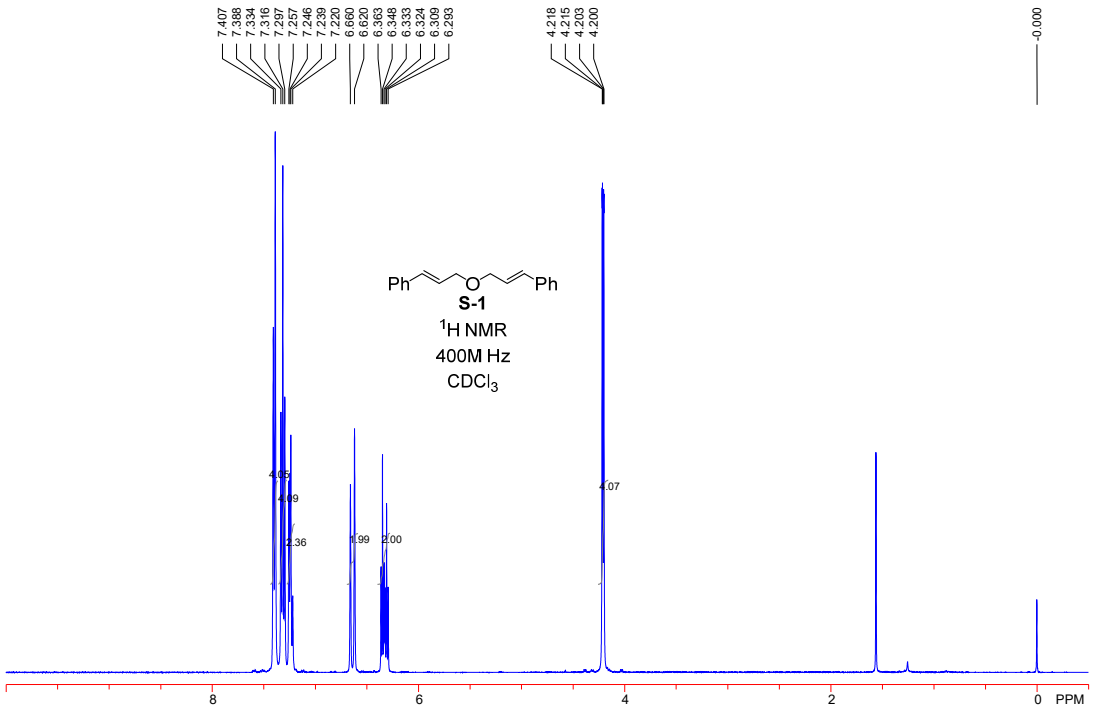

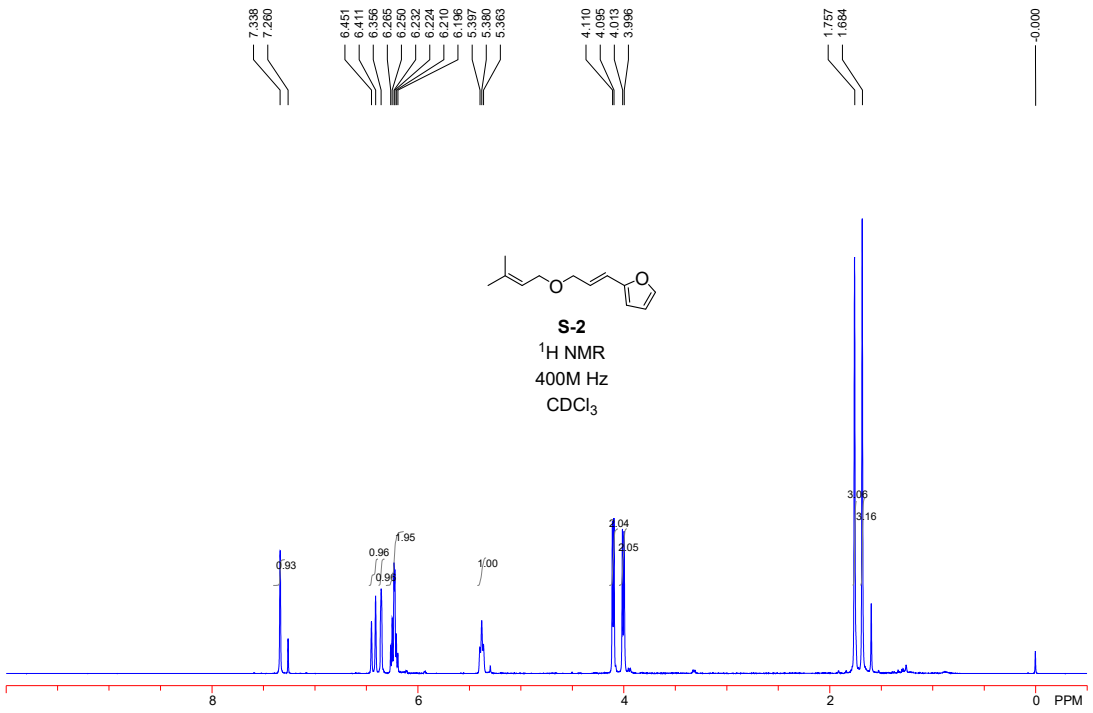

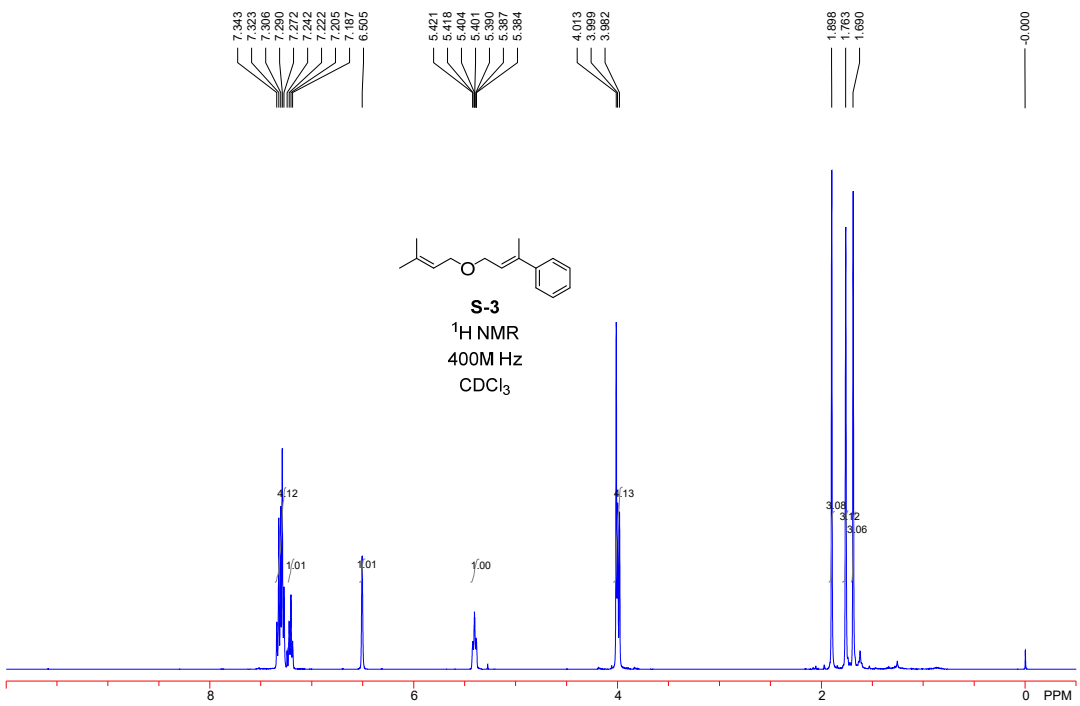
7.343
7.323
7.306
7.290
7.272
7.242
7.222
7.205
7.187
6.505
5.421
5.418
5.404
5.401
5.390
5.387
5.384
4.013
3.999
3.982
1.898
1.763
1.690
-0.000
S-3
1H NMR
400M Hz
CDCl3
4.12
1.01
1.01
1.00
4.13
3.08
3.12
3.06
8
6
4
2
0
PPM

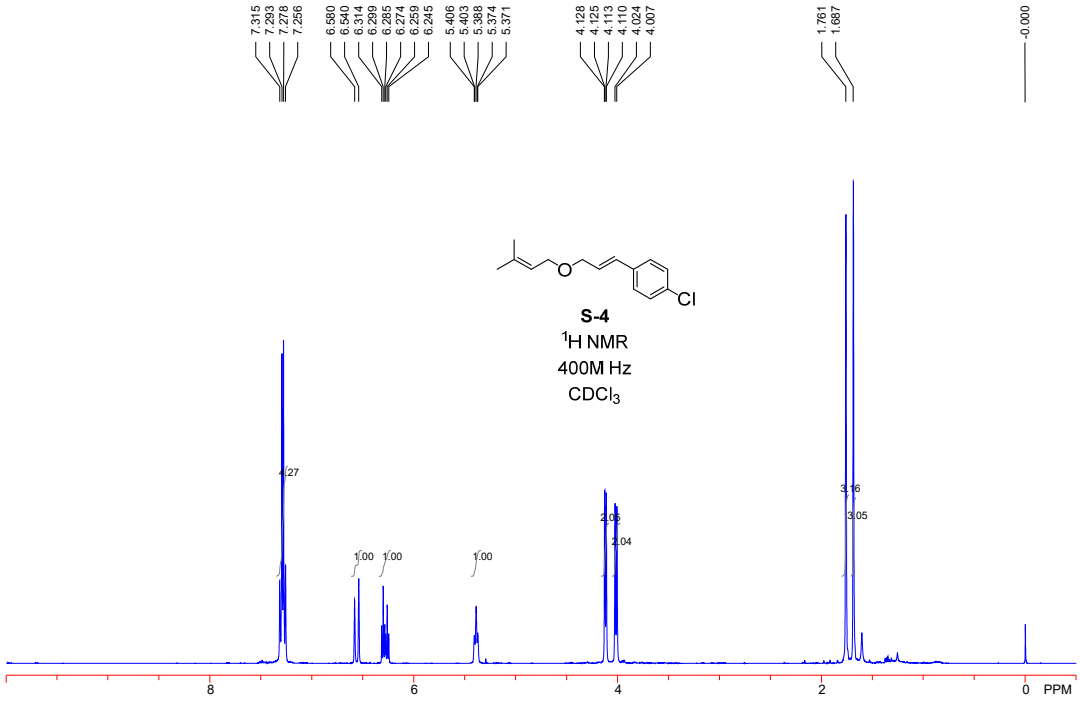
7.315
7.293
7.278
7.256
6.580
6.540
6.314
6.299
6.285
6.274
6.259
6.245
5.406
5.403
5.388
5.374
5.371
4.128
4.125
4.113
4.110
4.024
4.007
1.761
1.687
-0.000
Cl
S-4
1H NMR
400M Hz
CDCl3
4.27
1.00
1.00
1.00
2.05
2.04
3.16
3.05
8
6
4
2
0
PPM

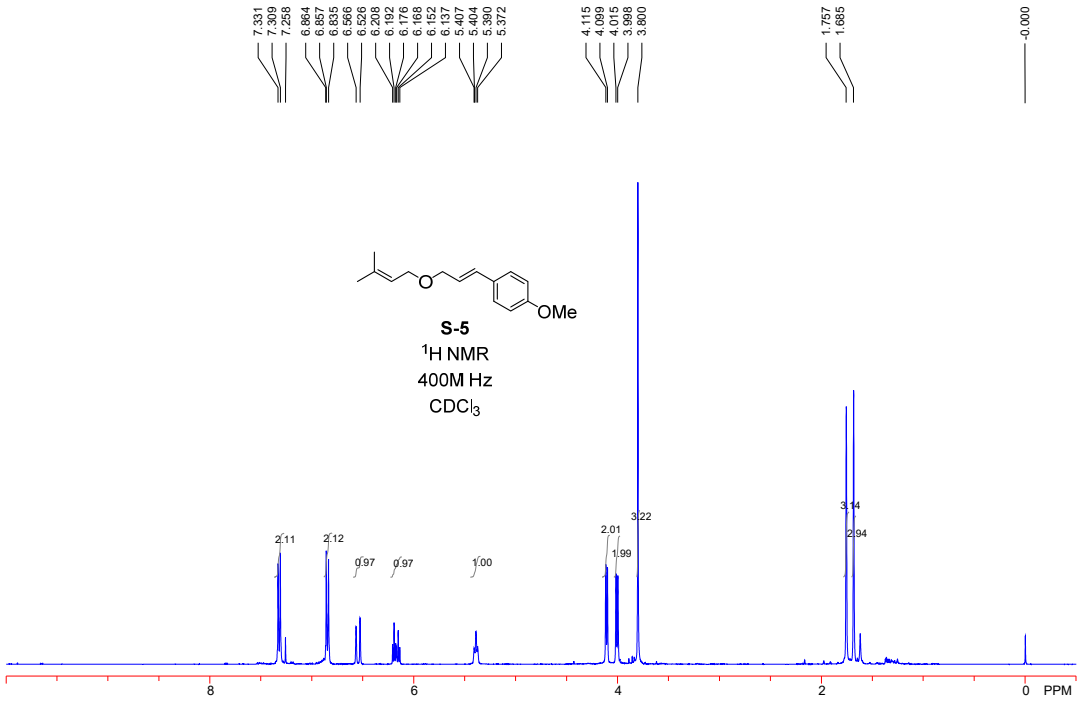
7.331
7.309
7.258
6.864
6.857
6.835
6.566
6.526
6.208
6.192
6.176
6.168
6.152
6.137
5.407
5.404
5.390
5.372
4.115
4.099
4.015
3.998
3.800
1.757
1.685
-0.000
O
OMe
S-5
1H NMR
400M Hz
CDCl3
2.11
2.12
0.97
0.97
1.00
2.01
1.99
3.22
3.14
2.94
8
6
4
2
0
PPM

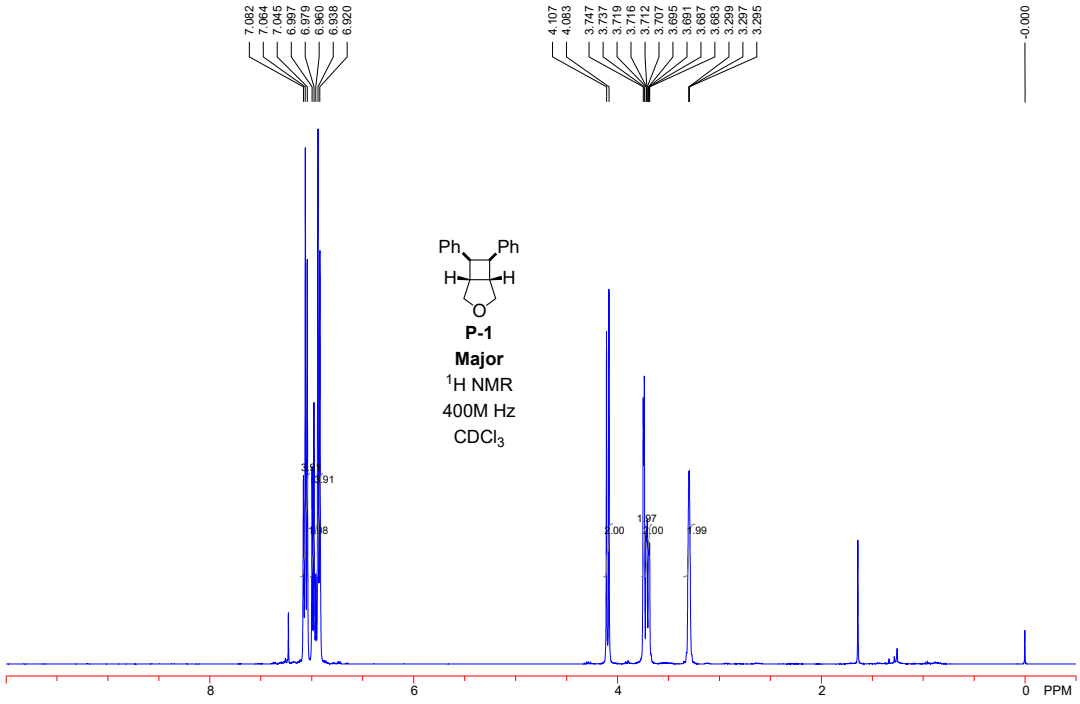
7.082
7.064
7.045
6.997
6.979
6.960
6.938
6.920
4.107
4.083
3.747
3.737
3.719
3.716
3.712
3.707
3.695
3.691
3.687
3.683
3.299
3.297
3.295
-0.000
Ph
Ph
H
H
O
P-1
Major
1H NMR
400M Hz
CDCl3
3.91
1.98
2.00
1.97
2.00
1.99
8
6
4
2
0
PPM

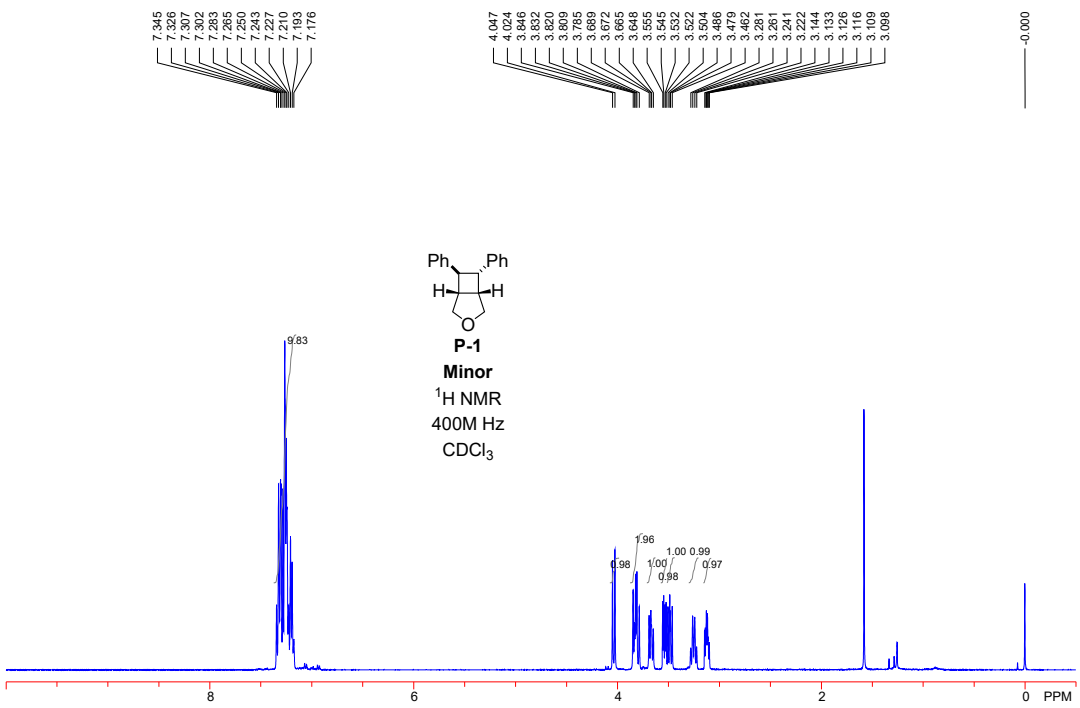
7.345
7.326
7.307
7.302
7.283
7.265
7.250
7.243
7.227
7.210
7.193
7.176
4.047
4.024
3.846
3.832
3.820
3.809
3.785
3.699
3.672
3.665
3.648
3.555
3.545
3.532
3.522
3.504
3.486
3.479
3.462
3.261
3.241
3.222
3.144
3.133
3.126
3.116
3.109
3.098
-0.000
Ph
Ph
H
H
O
P-1
Minor
1H NMR
400M Hz
CDCl3
9.83
1.96
1.00
0.99
0.98
1.00
0.98
0.97
8
6
4
2
0
PPM

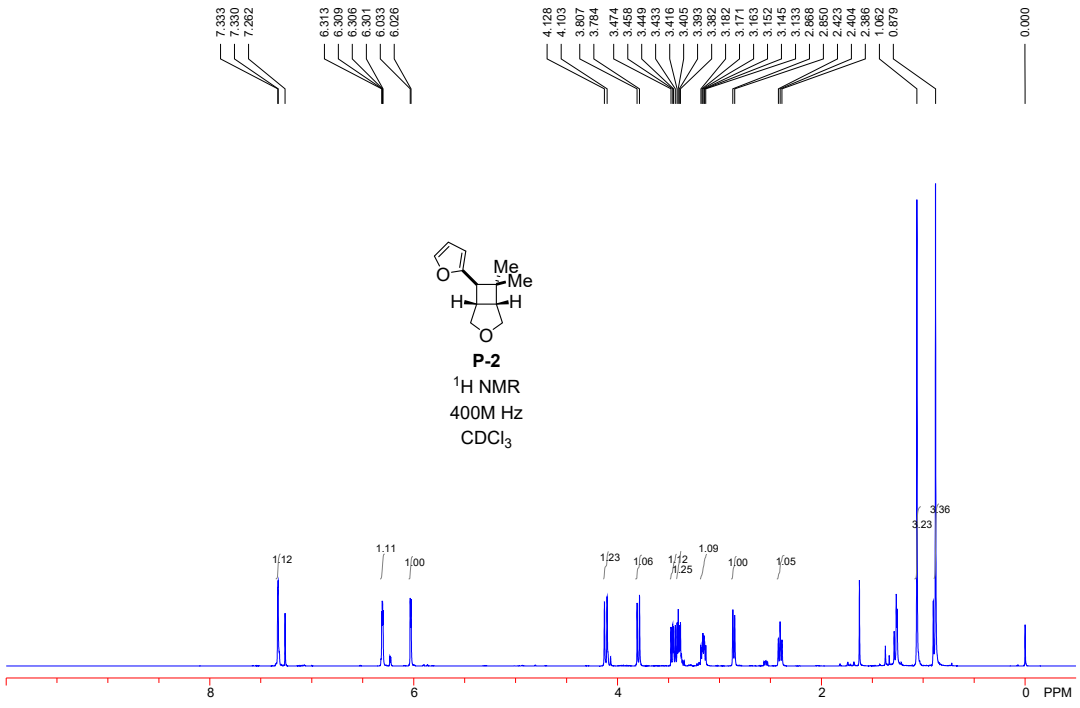
7.333
7.330
7.262
6.313
6.309
6.306
6.301
6.033
6.026
4.128
4.103
3.807
3.784
3.474
3.458
3.449
3.433
3.416
3.405
3.393
3.382
3.182
3.171
3.163
3.152
3.145
3.133
2.868
2.850
2.423
2.404
2.386
1.062
0.879
0.000
Me
Me
O
H
H
O
P-2
1H NMR
400M Hz
CDCl3
1.12
1.11
1.00
1.23
1.06
1.12
1.25
1.09
1.00
1.05
3.36
3.23
8
6
4
2
0
PPM

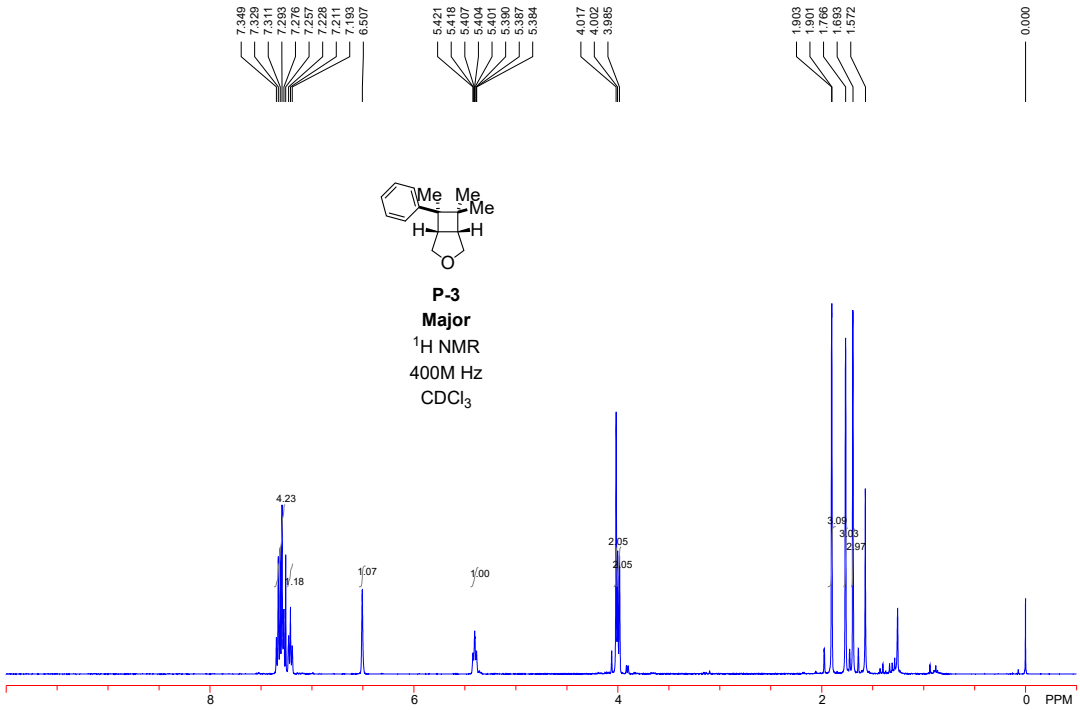
7.349
7.329
7.311
7.293
7.276
7.257
7.228
7.211
7.193
6.507
5.421
5.418
5.407
5.404
5.401
5.390
5.387
5.384
4.017
4.002
3.985
1.903
1.901
1.766
1.693
1.572
0.000
Me
Me
Me
H
H
O
P-3
Major
1H NMR
400M Hz
CDCl3
4.23
1.18
1.07
1.00
2.05
2.05
3.05
3.03
2.97
8
6
4
2
0
PPM

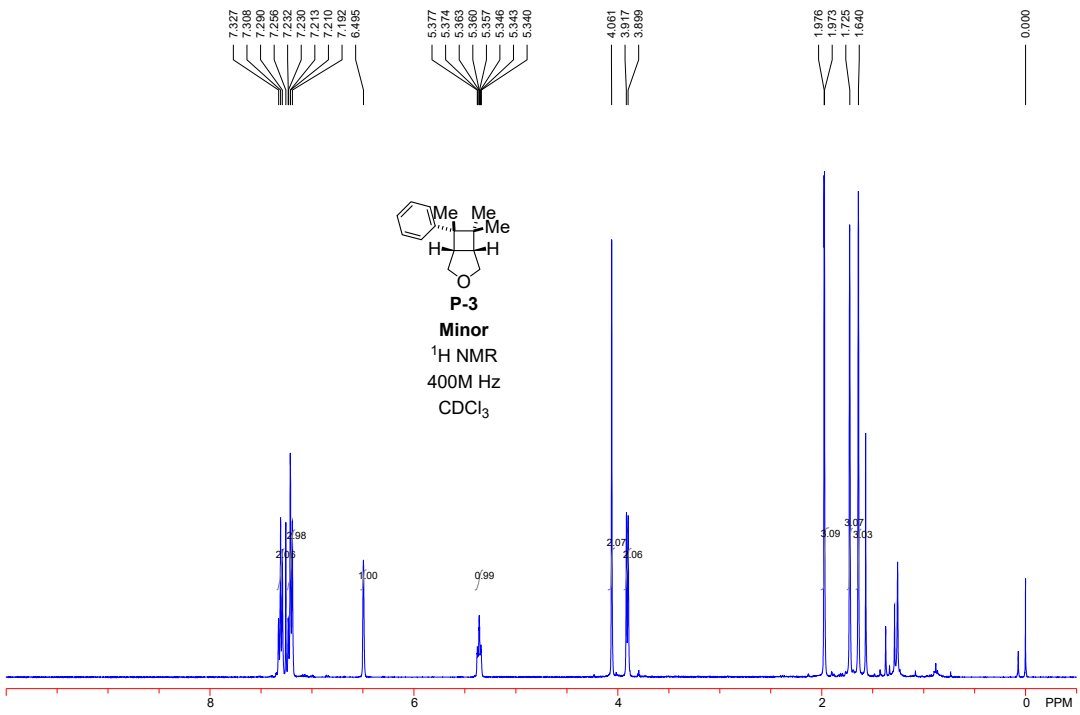
7.327
7.308
7.290
7.256
7.232
7.230
7.213
7.210
7.192
6.495
5.377
5.374
5.363
5.360
5.357
5.346
5.343
5.340
4.061
3.917
3.899
1.976
1.973
1.725
1.640
0.000
Me
Me
Me
H
H
O
P-3
Minor
1H NMR
400M Hz
CDCl3
2.98
2.08
1.00
0.99
2.07
2.06
3.09
3.07
3.03
8
6
4
2
0
PPM

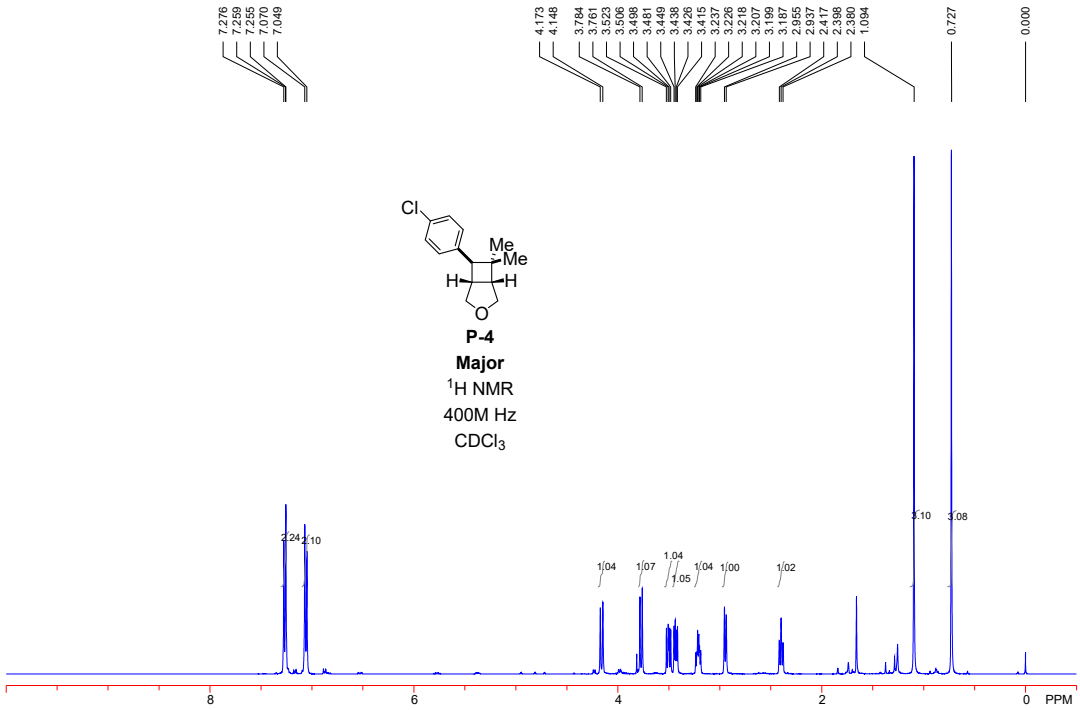
7.276
7.259
7.255
7.070
7.049
4.173
4.148
3.784
3.761
3.523
3.506
3.498
3.481
3.449
3.438
3.426
3.415
3.237
3.226
3.218
3.207
3.199
3.187
2.955
2.937
2.417
2.398
2.380
1.094
0.727
0.000
Cl
Me
Me
H
H
O
P-4
Major
1H NMR
400M Hz
CDCl3
2.24
2.10
1.04
1.07
1.04
1.05
1.04
1.00
1.02
3.10
3.08
8
6
4
2
0
PPM

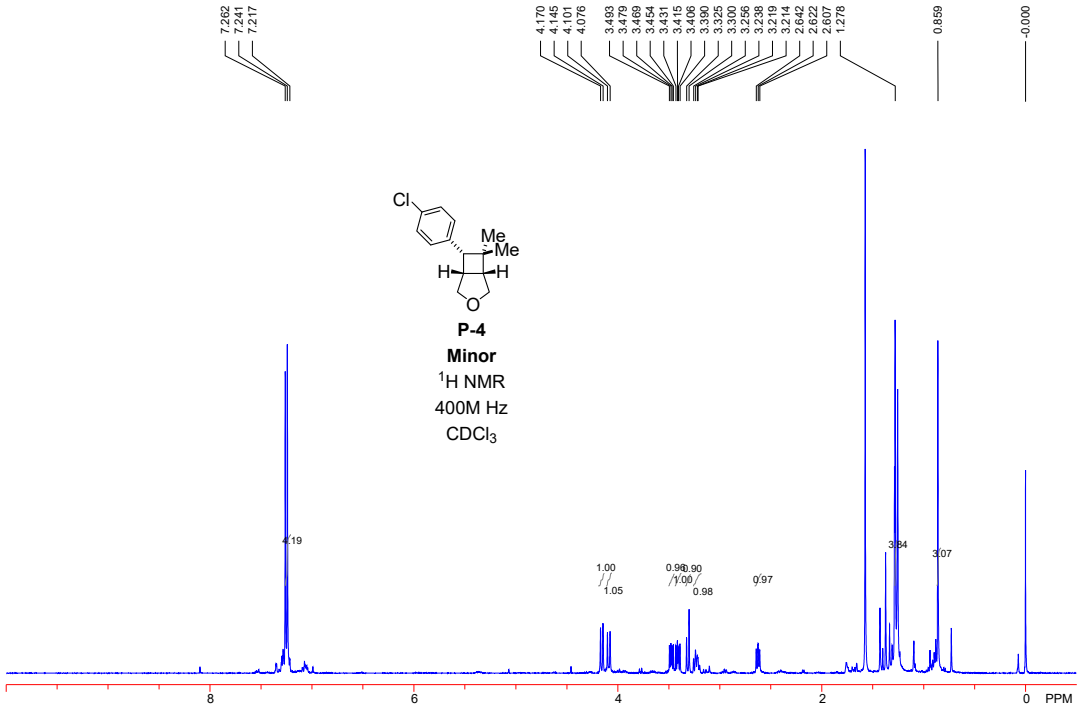
7.262
7.241
7.217
4.170
4.145
4.101
4.076
3.493
3.479
3.469
3.454
3.431
3.415
3.406
3.390
3.325
3.300
3.256
3.238
3.219
3.214
2.642
2.622
2.607
1.278
0.859
-0.000
Cl
Me
Me
H
H
O
P-4
Minor
1H NMR
400M Hz
CDCl3
4.19
1.00
1.05
0.96
1.00
0.90
0.98
0.97
3.84
3.07
8
6
4
2
0
PPM

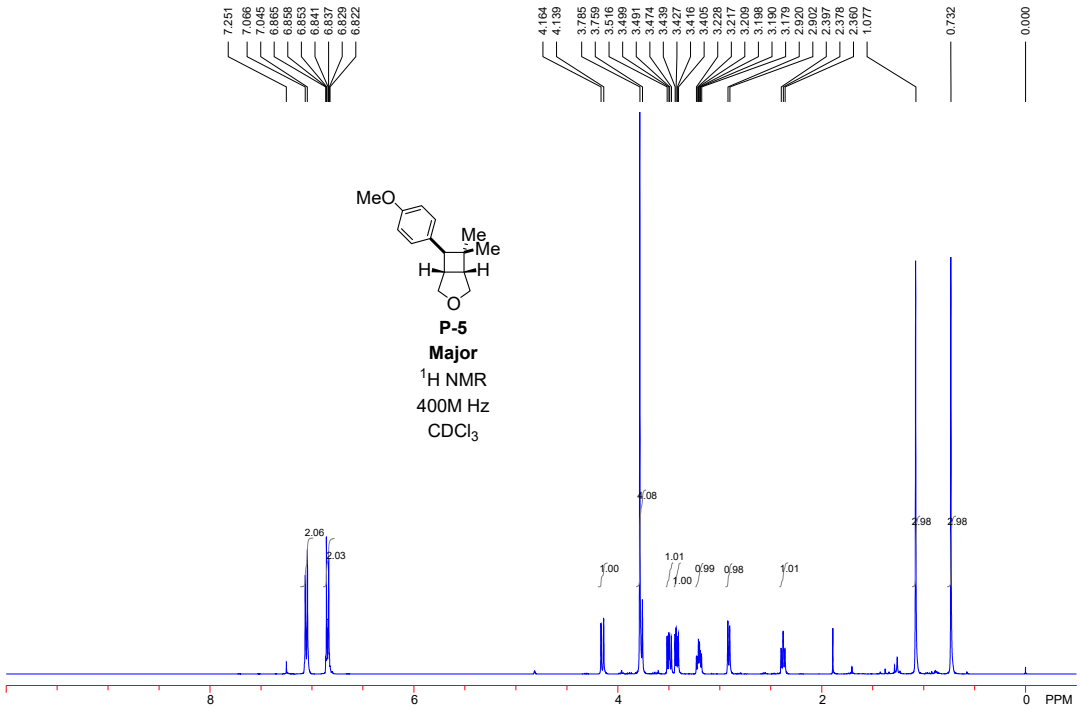
7.251
7.066
7.045
6.865
6.858
6.853
6.841
6.837
6.829
6.822
4.164
4.139
3.785
3.759
3.516
3.499
3.491
3.474
3.439
3.427
3.416
3.405
3.228
3.217
3.209
3.198
3.190
3.179
2.920
2.902
2.397
2.378
2.360
1.077
0.732
0.000
MeO
Me
Me
H
H
O
P-5
Major
1H NMR
400M Hz
CDCl3
2.06
2.03
4.08
1.00
1.01
1.00
0.99
0.98
1.01
2.98
2.98
8
6
4
2
0
PPM

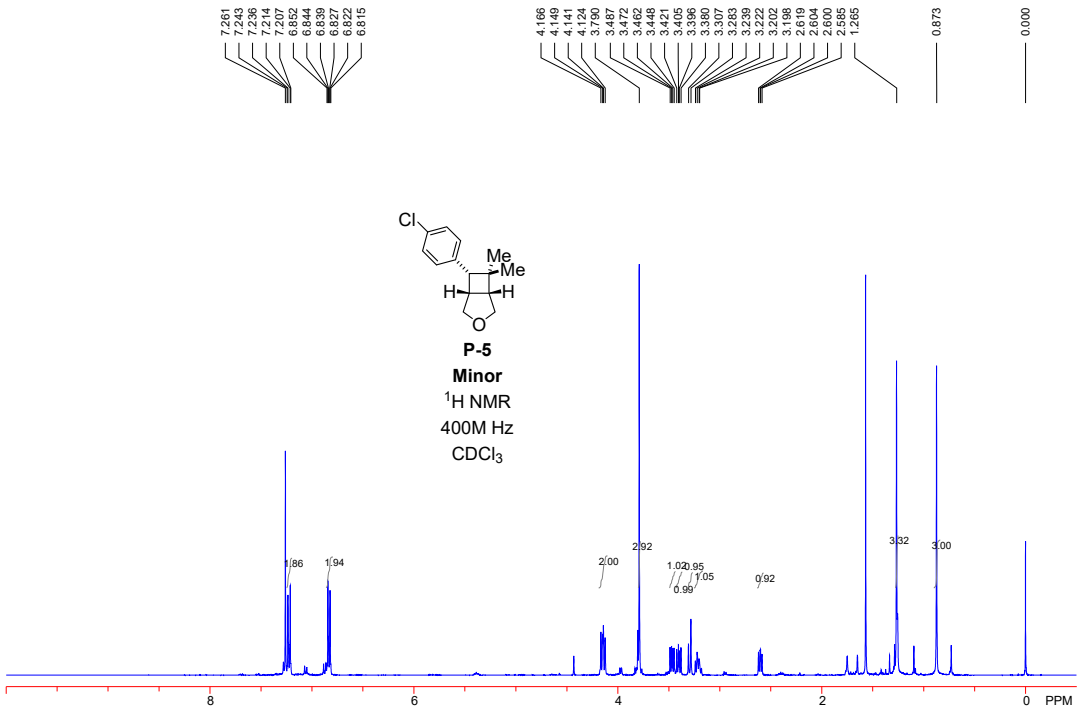
7.261
7.243
7.236
7.214
7.207
6.852
6.844
6.839
6.827
6.822
6.815
4.166
4.149
4.141
4.124
3.790
3.487
3.472
3.462
3.448
3.421
3.405
3.396
3.380
3.307
3.283
3.239
3.222
3.202
3.198
2.619
2.604
2.600
2.585
1.265
0.873
0.000
Cl
Me
Me
H
H
O
P-5
Minor
1H NMR
400M Hz
CDCl3
1.86
1.94
2.00
2.92
1.02
0.95
1.05
0.99
0.92
3.32
3.00
8
6
4
2
0
PPM

13. References

1. Lu, Z. & Yoon, T. P. Visible light photocatalysis of 2+2 styrene cycloadditions by energy transfer. *Angewandte Chemie-International Edition* **51**, 10329-10332 (2012).
2. Leitch, J. A., Rogova, T., Duarte, F. & Dixon, D. J. Dearomative Photocatalytic Construction of Bridged 1, 3-Diazepanes, *Angew. Chem. Int. Ed.* **59**, 4121–4130 (2020).
3. Miller, D. C. *et al.* Anti-Markovnikov hydroamination of unactivated alkenes with primary alkyl amines, *J. Am. Chem. Soc.* **141**, 16590–16594 (2019).
4. Primer, D. N., Karakaya, I., Tellis, J. C. & Molander, G. A. Single-electron transmetalation: an enabling technology for secondary alkylboron cross-coupling, *J. Am. Chem. Soc.* **137**, 2195–2198 (2015).
5. Ladouceur, S., Fortin, D. & Zysman-Colman, E. Enhanced luminescent iridium (III) complexes bearing aryltriazole cyclometallated ligands, *Inorg. Chem.* **50**, 11514–11526 (2011).
6. Tamayo, A. B. *et al.* Synthesis and characterization of facial and meridional tris-cyclometalated iridium (III) complexes, *J. Am. Chem. Soc.* **125**, 7377–7387 (2003).